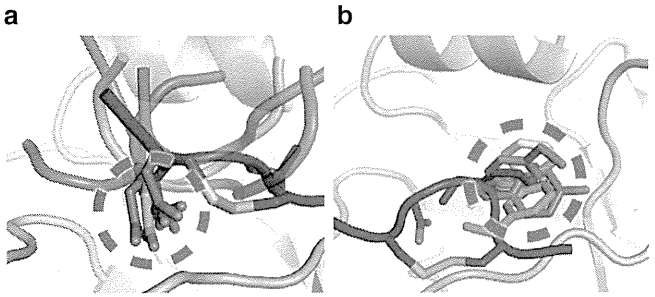

Figure 5 | Common trends in recognition of the HA by receptor-binding-site-targeted antibodies. (**a**) Antibodies HC19 (red, PDB 2VIR), HC63 (light blue, PDB 1KEN), CH65 (green, PDB 3SM5) and 5J8 (orange, PDB 4M5Z) use an Asp residue to insert a carboxylate in the receptor-binding site that would be occupied by the carboxylate of sialic acid of the α2,6 sialoglycan receptor (dashed red circle). (**b**) Antibodies HC19 (red, PDB 2VIR), C05 (yellow, PDB 4FP8), 8F8 (blue, PDB 4HF5), 8M2 (pink, PDB 4HFU) and 2G1 (green, PDB 4HG4) use hydrophobic residues to target the receptor-binding site that would be occupied by the acetamide moiety of sialic acid (dashed blue circle). The disulphide loop of the F045-092 HCDR3 is shown and coloured purple.

particularly in strains that appeared around and after 2003 and, in accord, the F045–092 Fab exhibits weaker binding for these more recent H3 strains (Table 1). However, the antibody binding appears to be tuned such that weaker Fab binding can be enhanced and accommodated by avidity of the bivalent IgG so as to extend the antibody's breadth of recognition, as observed with some other receptor-binding-site-targeted antibodies[15–17]. In addition, F045–092 appears to use slightly different approach angles to bind the Vic1975/H3 and Vic2011/H3 HAs, pivoting around the receptor-binding site likely to accommodate variable epitope residues. Altogether, these binding features allow F045–092 to have exceptional binding breadth against the entire H3 subtype as well as strains from the H1, H2 and H13 subtypes.

Common trends of recognition, as seen with F045–092 and other antibodies, are now emerging that show recurring modes of binding to attain broad recognition of the receptor-binding site. For instance, the use of receptor mimicry has been observed in other antibodies that similarly insert their HCDR3 into the HA receptor-binding site, which all use an Asp carboxylate at the tip of the loop to mimic the carboxylate of sialic acid[12,13,15,44,45]. These findings suggest that receptor mimicry of the carboxylate may be important for broad recognition of HA, which is utilized by half of the receptor-binding-site-targeted antibodies solved in complex with HAs to date (Fig. 5a), although other antibodies recognize this portion of the receptor-binding site by other means[14,16,17,23]. In addition, nearly all receptor-binding-site-targeted antibodies commonly insert a hydrophobic residue into the universally conserved hydrophobic pocket formed by Trp153 and Leu194 that would be occupied by the acetamide moiety of sialic acid. The identity of this hydrophobic residue can vary from a smaller residue, such as proline or valine, to a bulky aromatic residue, such as tyrosine, phenylalanine or tryptophan (Fig. 5b). Among the structurally characterized receptor-binding-site-targeted antibodies, F045–092 most closely resembles C05 as both antibodies contact a very small HA footprint primarily through their long HCDR3 loops[16]. In contrast, these antibodies differ in their angle of approach by ~113° (Supplementary Fig. 6) and the interaction of C05 with HA does not resemble those of the receptor, suggesting that there is considerable versatility in targeting the receptor-binding site.

The crystal structures of F045–092 in complex with divergent HAs reveal that the receptor-binding site is a hotspot for antibody recognition and is a key site of vulnerability against influenza HA. The challenge now is how the information gained from these structures can be applied to inform the design of improved vaccines or broad-spectrum small-molecule therapeutics, which are currently unavailable as a countermeasure against influenza HA. For instance, multimerization of the HA heads onto a self-assembling platform in combination with epitope focusing of the receptor-binding site may elicit a greater antibody response as an alternative vaccination strategy[46,47]. Since F045–092 only uses its V_H domain to contact a very minimal epitope on HA, it may be a promising candidate as a nanobody therapeutic or a diagnostic against H3 viruses[48,49]. Owing to its extremely small footprint on HA, another possibility may be to computationally design small proteins to bind the receptor-binding site, as previously achieved for the HA stem[50,51]. However, the synthesized F045–092 HCDR3 peptide does not compete with Fab binding nor could it be co-crystallized with HA, suggesting that the antibody stabilizes the proper conformation of the antibody HCDR3 loop by utilizing contacts from the other HCDRs, as also seen for the C05 antibody[16].

Although the ultimate goal is for universal therapy against all flu viruses, it may be more practical to also focus attention on the H1, H3 and flu B viruses that currently circulate in humans and have been responsible for all recent pandemics, epidemics and seasonal flu in the last 46 years. No previous antibody has been able to achieve complete HA subtype recognition at the receptor-binding site as described and characterized here for F045–092, and the structural information has great potential to serve as a template for the design of next-generation therapeutics against all H3 influenza viruses.

Methods

Fab and IgG expression and purification. F045–092 Fab and Fab mutants ($His^{H100a}Ala$; $Cys^{H100c}Ala$, $Cys^{H100f}Ala$; $Leu^{H100d}Ala$; $Asp^{H100e}Ala$) were individually cloned into the pFastBac Dual vector (Invitrogen) with N-terminal gp67 signal peptides fused to the light and heavy chains and a C-terminal His_6 tag fused to the heavy chain. Recombinant bacmid DNA was generated using the Bac-to-Bac system (Invitrogen) and baculovirus was generated by transfecting purified bacmid DNA into Sf9 cells using Cellfectin II (Invitrogen). F045–092 Fab and mutants were expressed by infecting suspension cultures of High Five cells (Invitrogen) with baculovirus shaking at 110 r.p.m. for 72 h at 28 °C. The proteins were purified by Ni-NTA (Qiagen), protein G, Mono S chromatography (GE Healthcare), followed by a final step of gel filtration (GE Healthcare).

F045–092 Fab was also prepared in *E. coli* DH12S cells (Invitrogen). C-terminal His_6 and FLAG tags were fused to the heavy and light chains, respectively. DH12S cells harbouring the F045–092 Fab expression plasmids were cultured in 2 × YT medium at 30 °C and induced with 1 mM IPTG at an optical density of 0.7 overnight. The culture supernatant was recovered and subjected to 60% ammonium sulphate precipitation. The precipitant was dissolved in PBS and the Fab was purified by Ni-NTA (Qiagen), anti-FLAG antibody M2 (Sigma), Mono S chromatography (GE Healthcare), followed by a final step of gel filtration (GE Healthcare).

To generate F045–092 IgG, the antibody light and heavy chains were each cloned into a modified pCAGGS vector[52] containing a dihydrofolate reductase (DHFR) gene. CHO (DHFR −) cells were co-transfected with the resultant plasmids and cultured in serum-free media. F045–092 IgG was purified from the culture supernatant by Capto Q chromatography (GE Healthcare) and Protein A affinity chromatography (ProteNova).

HA expression and purification. Baculovirus-expressed HA was prepared for binding studies and crystallization. Briefly, each HA was fused with an N-terminal gp67 signal peptide and a C-terminal BirA biotinylation site, thrombin cleavage site, trimerization domain and a His_6 tag. The HAs were expressed, as described above for the F045–092 Fabs, as either HA0 (human HAs) or mature HA (HA1/HA2; due to the polybasic linker in avian HAs between HA1 and HA2) and purified by Ni-NTA (Qiagen). For crystallization, the HA0 of Vic1975/H3 was treated with trypsin (NEB) to remove the C-terminal foldon and His_6 tags and to produce mature HA. The HA was then purified by a final step of gel filtration (GE Healthcare). For binding studies, each HA0 or mature HA was biotinylated with BirA and purified by gel filtration (GE Healthcare). The biotinylation reactions contained 100 mM Tris (pH 8.0), 10 mM ATP, 10 mM magnesium acetate, 50 μM biotin and <50 mM NaCl, and were incubated at 37 °C for 1–2 h.

K_d determination. K_d values were determined by bio-layer interferometry using an Octet RED instrument (ForteBio, Inc.). Biotinylated HAs at ~10–50 μg ml^{-1} in 1 × kinetics buffer (1 × PBS (pH 7.4), 0.01% BSA and 0.002% Tween 20) were immobilized onto streptavidin-coated biosensors and incubated with varying concentrations of baculovirus-expressed F045–092 Fab or IgG. All binding data were collected at 30 °C. The k_{on} and k_{off} values of each Fab and IgG were measured in real-time to determine K_d values for each Fab and IgG for each HA tested. The sequences of the HA proteins used in the binding studies and the experimental binding curves for each Fab and IgG for fitting k_{on} and k_{off} are reported in Supplementary Fig. 7. The sequences of all biotinylated HAs used in this work are available in FASTA format in the Supplementary Methods.

Crystallization and structural determination of Fab F045-092. Bacterially expressed F045–092 Fab crystals were grown by sitting-drop vapour diffusion at 20 °C by mixing 0.75 μl of concentrated protein sample (7.3 mg ml^{-1}) with 0.75 μl of mother liquor (30% PEG 600, 0.1 M phosphate-citrate, pH 5.0). Crystals appeared in 7 days and were cryoprotected with mother liquor supplemented with 20% ethylene glycol. X-ray diffraction data were collected to 1.50 Å resolution at beamline 11-1 (wavelength 0.97945 Å) at the Stanford Synchrotron Radiation Lightsource (SSRL) and were processed in space group $P2_12_12_1$ using XDS[53]. The structure was determined by molecular replacement with Phaser[54] using the variable and constant domains of Fab New (PDB 7FAB (ref. 55)) as search models and one Fab was found in the asymmetric unit. The model was iteratively rebuilt using Coot[56] and refined in Phenix[57]. Refinement parameters include initial rigid-body refinement (each Ig domain) and simulated annealing followed by restrained refinement including TLS refinement (each Ig domain as a TLS group). In the final F045–092 Fab structure, 97.9% of the residues are in favored regions of the Ramachandran plot with 0% outliers, as calculated by MolProbity[58].

Crystallization and structural determination of the Vic2011/H3 HA. EndoH-treated baculovirus-expressed Vic2011/H3 HA was crystallized by sitting-drop vapour diffusion at 4 °C by mixing 0.75 μl of concentrated protein sample (3 mg ml^{-1}) with 0.75 μl of mother liquor (5% PEG 8000, 20% PEG 300, 10% glycerol, 0.1 M Tris, pH 8.7). Crystals appeared in 3 days. X-ray diffraction data were collected to 1.75 Å resolution at SSRL beamline 11-1 (wavelength 0.97945 Å) and were processed in space group H32 using XDS[53]. The structure was determined by molecular replacement with Phaser[54] using a protomer of the apo 2005 Hong Kong (H3N2) HA (PDB 2YP7 (ref. 43)) as the search model. One HA protomer (HA1/HA2) of the HA trimer was found in the asymmetric unit. The model was iteratively rebuilt using Coot[56] and refined in Phenix[57]. Refinement parameters include initial rigid-body refinement and simulated annealing followed by restrained refinement including TLS refinement (each HA1 and HA2 chain). In the final Vic2011/H3 HA structure, 96.6% of the residues are in favored regions of the Ramachandran plot with 0% outliers[58].

Crystallization and structural determination of F045-092 Fab-HA complexes. For Fab–HA complex formation, baculovirus-expressed Fab F045–092 was added to Vic1975/H3 or Vic2011/H3 HA in a molar ratio of 3.2:1 to achieve 3 Fabs per HA trimer, incubated at room temperature for 1 h and the complex was then purified from unbound Fab by gel filtration. F045–092–Vic1975/H3 crystals were grown by sitting drop vapour diffusion at 4 °C by mixing 0.75 μl of concentrated protein sample (5.7 mg ml^{-1}) with 0.75 μl of mother liquor (1.7 M ammonium sulphate, 0.1 M Tris (pH 8.1), 4% PEG 400). Crystals appeared in 7 days and were cryoprotected with mother liquor supplemented with increasing concentrations of glycerol (5% steps, 10 min per step) to a final concentration of 25%. X-ray diffraction data were collected to 2.75 Å resolution at the GM/CA CAT 23ID-B beamline (wavelength 1.03322 Å) at the Advanced Photon Source (APS) and were processed in space group P321 using XDS[53]. The structure was determined by molecular replacement with Phaser[54], using the variable domain of the high-resolution Fab structure and the HA protomer of Vic1975/H3 (PDB 4GMS (ref. 17), chains A and B) as models. After rigid-body refinement of the HA and Fab variable domain, density was observed for the constant domain, which was docked in by hand and refined using rigid-body refinement. The model was iteratively rebuilt using Coot[56] and refined in Phenix[57]. Refinement parameters include rigid-body refinement (each Ig domain and HA protomer) and simulated annealing followed by restrained refinement including TLS refinement (each Ig domain and HA chain). In the final F045–092–Vic1975/H3 structure, 96.2% of the residues are in favored regions of the Ramachandran plot with 0.3% outliers[58].

F045–092–Vic2011/H3 crystals were grown by sitting-drop vapour diffusion at 20 °C by mixing 0.75 μl of concentrated protein sample (9.1 mg ml^{-1}) with 0.75 μl of mother liquor (20% PEG 400, 30% 1,2-propanediol, 0.1 M HEPES, pH 7.5). Crystals appeared in 7 days. X-ray diffraction data were collected to 6.50 Å resolution at the GM/CA CAT 23ID-B beamline (wavelength 1.03318 Å) at APS and were processed in space group C2 using XDS[53]. The structure was determined by molecular replacement with Phaser[54] using the high-resolution apo A/Victoria/361/2011 (H3N2) HA trimer as a search model to locate two HA trimers in the asymmetric unit. Next, six copies of the variable domain of the high-resolution F045–092 Fab structure were used as search models after fixing the position and orientation of the two HA trimers but only five variable domain copies were found. After rigid-body refinement, density was observed for the remaining Fab variable and constant domains, which were then docked in by hand and refined with rigid-body refinement. The model was iteratively rebuilt using Coot[56] and refined in Phenix[57] using the high-resolution Fab and HA structures to generate reference model restraints and with similar parameters as in the F045–092–Vic1975/H3 complex. In the final F045–092–Vic2011/H3 structure, 97.4% of the residues are in favored regions of the Ramachandran plot with 0% outliers[58]. The data were processed and the structure was refined in a C2 space group but exhibited pseudosymmetry that resembled the symmetry in space group P321. However, the C2 space group appeared to be the correct choice and also had better statistics and better density, especially for some of the carbohydrate moieties.

Structural analyses. Hydrogen bonds and van der Waals contacts were calculated using HBPLUS[59] and CONTACSYM[60], respectively. Molecular surface area buried upon Fab binding was calculated using MS[61]. MacPyMol (DeLano Scientific) was used to render structure figures. Kabat numbering was applied to the variable domains of the Fabs using the AbNum server[62]. The final coordinates were validated using the JCSG quality control server (v2.8), which includes MolProbity[58].

Sequence analysis of F045-092 epitope conservation. All full-length and non-redundant human influenza A HA sequences were downloaded on 12 December 2013 from the Influenza Virus Resource at the NCBI database[63]. The sequences were aligned using MUSCLE[64] and analysed using GCG (Accelrys) and custom shell scripts (available from the authors upon request).

References

1. CDC. Update: influenza activity—United States, September 30, 2012–February 9, 2013. *MMWR Morb. Mortal. Wkly. Rep.* **62,** 124–130 (2013).
2. Le, Q. M. *et al.* Avian flu: isolation of drug-resistant H5N1 virus. *Nature* **437,** 1108 (2005).
3. Stephenson, I. *et al.* Neuraminidase inhibitor resistance after oseltamivir treatment of acute influenza A and B in children. *Clin. Infect. Dis.* **48,** 389–396 (2009).
4. Gao, R. *et al.* Human infection with a novel avian-origin influenza A (H7N9) virus. *New Engl. J. Med.* **368,** 1888–1897 (2013).
5. Cohen, J. Influenza. New flu virus in China worries and confuses. *Science* **340,** 129–130 (2013).
6. Wilson, I. A., Skehel, J. J. & Wiley, D. C. Structure of the haemagglutinin membrane glycoprotein of influenza virus at 3 Å resolution. *Nature* **289,** 366–373 (1981).
7. Weis, W. *et al.* Structure of the influenza virus haemagglutinin complexed with its receptor, sialic acid. *Nature* **333,** 426–431 (1988).
8. Zhu, X. *et al.* Hemagglutinin homologue from H17N10 bat influenza virus exhibits divergent receptor-binding and pH-dependent fusion activities. *Proc. Natl Acad. Sci. USA* **110,** 1458–1463 (2013).
9. Sun, X. *et al.* Bat-derived influenza hemagglutinin H17 does not bind canonical avian or human receptors and most likely uses a unique entry mechanism. *Cell Rep.* **3,** 769–778 (2013).
10. Tong, S. *et al.* New world bats harbor diverse influenza A viruses. *PLoS Pathog.* **9,** e1003657 (2013).
11. Bullough, P. A., Hughson, F. M., Skehel, J. J. & Wiley, D. C. Structure of influenza haemagglutinin at the pH of membrane fusion. *Nature* **371,** 37–43 (1994).
12. Whittle, J. R. *et al.* Broadly neutralizing human antibody that recognizes the receptor-binding pocket of influenza virus hemagglutinin. *Proc. Natl Acad. Sci. USA* **108,** 14216–14221 (2011).
13. Schmidt, A. G. *et al.* Preconfiguration of the antigen-binding site during affinity maturation of a broadly neutralizing influenza virus antibody. *Proc. Natl Acad. Sci. USA* **110,** 264–269 (2013).
14. Xu, R. *et al.* A recurring motif for antibody recognition of the receptor-binding site of influenza hemagglutinin. *Nat. Struct. Mol. Biol.* **20,** 363–370 (2013).
15. Hong, M. *et al.* Antibody recognition of the pandemic H1N1 influenza hemagglutinin receptor binding site. *J. Virol.* **87,** 12471–12480 (2013).
16. Ekiert, D. C. *et al.* Cross-neutralization of influenza A viruses mediated by a single antibody loop. *Nature* **489,** 526–532 (2012).
17. Lee, P. S. *et al.* Heterosubtypic antibody recognition of the influenza virus hemagglutinin receptor binding site enhanced by avidity. *Proc. Natl Acad. Sci. USA* **109,** 17040–17045 (2012).
18. Julien, J. P., Lee, P. S. & Wilson, I. A. Structural insights into key sites of vulnerability on HIV-1 Env and influenza HA. *Immunol. Rev.* **250,** 180–198 (2012).
19. Ohshima, N. *et al.* Naturally occurring antibodies in humans can neutralize a variety of influenza virus strains, including H3, H1, H2, and H5. *J. Virol.* **85,** 11048–11057 (2011).
20. Harris, A. *et al.* Influenza virus pleiomorphy characterized by cryoelectron tomography. *Proc. Natl Acad. Sci. USA* **103,** 19123–19127 (2006).

21. Ekiert, D. C. *et al.* Antibody recognition of a highly conserved influenza virus epitope. *Science* **324,** 246–251 (2009).
22. Corti, D. *et al.* A neutralizing antibody selected from plasma cells that binds to group 1 and group 2 influenza A hemagglutinins. *Science* **333,** 850–856 (2011).
23. Tsibane, T. *et al.* Influenza human monoclonal antibody 1F1 interacts with three major antigenic sites and residues mediating human receptor specificity in H1N1 viruses. *PLoS Pathog.* **8,** e1003067 (2012).
24. Stanfield, R. L., Zemla, A., Wilson, I. A. & Rupp, B. Antibody elbow angles are influenced by their light chain class. *J. Mol. Biol.* **357,** 1566–1574 (2006).
25. Wiley, D. C., Wilson, I. A. & Skehel, J. J. Structural identification of the antibody-binding sites of Hong Kong influenza haemagglutinin and their involvement in antigenic variation. *Nature* **289,** 373–378 (1981).
26. Sui, J. *et al.* Structural and functional bases for broad-spectrum neutralization of avian and human influenza A viruses. *Nat. Struct. Mol. Biol.* **16,** 265–273 (2009).
27. Almagro, J. C. *et al.* Characterization of a high-affinity human antibody with a disulfide bridge in the third complementarity-determining region of the heavy chain. *J. Mol. Recognit.* **25,** 125–135 (2012).
28. Kong, L. *et al.* Hepatitis C virus E2 envelope glycoprotein core structure. *Science* **342,** 1090–1094 (2013).
29. Ekiert, D. C. *et al.* A highly conserved neutralizing epitope on group 2 influenza A viruses. *Science* **333,** 843–850 (2011).
30. Dreyfus, C. *et al.* Highly conserved protective epitopes on influenza B viruses. *Science* **337,** 1343–1348 (2012).
31. Dreyfus, C., Ekiert, D. C. & Wilson, I. A. Structure of a classical broadly neutralizing stem antibody in complex with a pandemic H2 hemagglutinin. *J. Virol.* **87,** 7149–7154 (2013).
32. Friesen, R. H. *et al.* A common solution to group 2 influenza virus neutralization. *Proc. Natl Acad. Sci. USA* **111,** 450–455 (2014).
33. Skehel, J. J. *et al.* A carbohydrate side chain on hemagglutinins of Hong Kong influenza viruses inhibits recognition by a monoclonal antibody. *Proc. Natl Acad. Sci. USA* **81,** 1779–1783 (1984).
34. Abe, Y. *et al.* Effect of the addition of oligosaccharides on the biological activities and antigenicity of influenza A/H3N2 virus hemagglutinin. *J. Virol.* **78,** 9605–9611 (2004).
35. Wang, C. C. *et al.* Glycans on influenza hemagglutinin affect receptor binding and immune response. *Proc. Natl Acad. Sci. USA* **106,** 18137–18142 (2009).
36. Xu, R. *et al.* Structural basis of preexisting immunity to the 2009 H1N1 pandemic influenza virus. *Science* **328,** 357–360 (2010).
37. Wei, C. J. *et al.* Cross-neutralization of 1918 and 2009 influenza viruses: role of glycans in viral evolution and vaccine design. *Sci. Transl. Med.* **2,** 24ra21 (2010).
38. Karlsson Hedestam, G. B. *et al.* The challenges of eliciting neutralizing antibodies to HIV-1 and to influenza virus. *Nat. Rev. Microbiol.* **6,** 143–155 (2008).
39. Pejchal, R. *et al.* A potent and broad neutralizing antibody recognizes and penetrates the HIV glycan shield. *Science* **334,** 1097–1103 (2011).
40. McLellan, J. S. *et al.* Structure of HIV-1 gp120 V1/V2 domain with broadly neutralizing antibody PG9. *Nature* **480,** 336–343 (2011).
41. Julien, J. P. *et al.* Asymmetric recognition of the HIV-1 trimer by broadly neutralizing antibody PG9. *Proc. Natl Acad. Sci. USA* **110,** 4351–4356 (2013).
42. Pancera, M. *et al.* Structural basis for diverse N-glycan recognition by HIV-1-neutralizing V1-V2-directed antibody PG16. *Nat. Struct. Mol. Biol.* **20,** 804–813 (2013).
43. Lin, Y. P. *et al.* Evolution of the receptor binding properties of the influenza A (H3N2) hemagglutinin. *Proc. Natl Acad. Sci. USA* **109,** 21474–21479 (2012).
44. Bizebard, T. *et al.* Structure of influenza virus haemagglutinin complexed with a neutralizing antibody. *Nature* **376,** 92–94 (1995).
45. Barbey-Martin, C. *et al.* An antibody that prevents the hemagglutinin low pH fusogenic transition. *Virology* **294,** 70–74 (2002).
46. Jardine, J. *et al.* Rational HIV immunogen design to target specific germline B cell receptors. *Science* **340,** 711–716 (2013).
47. Kanekiyo, M. *et al.* Self-assembling influenza nanoparticle vaccines elicit broadly neutralizing H1N1 antibodies. *Nature* **499,** 102–106 (2013).
48. Zhang, J. *et al.* Pentamerization of single-domain antibodies from phage libraries: a novel strategy for the rapid generation of high-avidity antibody reagents. *J. Mol. Biol.* **335,** 49–56 (2004).
49. Wesolowski, J. *et al.* Single domain antibodies: promising experimental and therapeutic tools in infection and immunity. *Med. Microbiol. Immunol.* **198,** 157–174 (2009).
50. Fleishman, S. J. *et al.* Computational design of proteins targeting the conserved stem region of influenza hemagglutinin. *Science* **332,** 816–821 (2011).
51. Whitehead, T. A. *et al.* Optimization of affinity, specificity and function of designed influenza inhibitors using deep sequencing. *Nat. Biotechnol.* **30,** 543–548 (2012).
52. Niwa, H., Yamamura, K. & Miyazaki, J. Efficient selection for high-expression transfectants with a novel eukaryotic vector. *Gene* **108,** 193–199 (1991).
53. Kabsch, W. XDS. *Acta Crystallogr. D Biol. Crystallogr.* **66,** 125–132 (2010).
54. McCoy, A. J. *et al.* Phaser crystallographic software. *J. Appl. Crystallogr.* **40,** 658–674 (2007).
55. Saul, F. A. & Poljak, R. J. Crystal structure of human immunoglobulin fragment Fab New refined at 2.0 Å resolution. *Proteins* **14,** 363–371 (1992).
56. Emsley, P., Lohkamp, B., Scott, W. G. & Cowtan, K. Features and development of Coot. *Acta Crystallogr. D Biol. Crystallogr.* **66,** 486–501 (2010).
57. Adams, P. D. *et al.* PHENIX: a comprehensive Python-based system for macromolecular structure solution. *Acta Crystallogr. D Biol. Crystallogr.* **66,** 213–221 (2010).
58. Chen, V. B. *et al.* MolProbity: all-atom structure validation for macromolecular crystallography. *Acta Crystallogr. D Biol. Crystallogr.* **66,** 12–21 (2010).
59. McDonald, I. K. & Thornton, J. M. Satisfying hydrogen bonding potential in proteins. *J. Mol. Biol.* **238,** 777–793 (1994).
60. Sheriff, S., Hendrickson, W. A. & Smith, J. L. Structure of myohemerythrin in the azidomet state at 1.7/1.3 Å resolution. *J. Mol. Biol.* **197,** 273–296 (1987).
61. Connolly, M. L. Analytical molecular surface calculation. *J. Appl. Crystallogr.* **16,** 548–558 (1983).
62. Abhinandan, K. R. & Martin, A. C. Analysis and improvements to Kabat and structurally correct numbering of antibody variable domains. *Mol. Immunol.* **45,** 3832–3839 (2008).
63. Bao, Y. *et al.* The influenza virus resource at the National Center for Biotechnology Information. *J. Virol.* **82,** 596–601 (2008).
64. Edgar, R. C. MUSCLE: multiple sequence alignment with high accuracy and high throughput. *Nucleic Acids Res.* **32,** 1792–1797 (2004).

Acknowledgements

We thank H. Tien of the Robotics Core at the Joint Center for Structural Genomics for automated crystal screening, the staff of the Advanced Photon Source (APS) GM/CA CAT beamline 23ID-B and the Stanford Synchrotron Radiation Lightsource (SSRL) beamline 11-1 for support, M. Elsliger (The Scripps Research Institute) and the instructors from the 2012 CCP4 School held at APS for crystallographic and computational support, and J.-P. Julien, X. Zhu (The Scripps Research Institute), and D.C. Ekiert (University of California, San Francisco) for helpful discussions. The work was funded in part by NIH grants R56 AI099275 (I.A.W.) and GM080209 for the NIH Molecular Evolution Training Program at TSRI (P.S.L.), and the Skaggs Institute for Chemical Biology. SSRL is a Directorate of SLAC National Accelerator Laboratory and an Office of Science User Facility operated for the US Department of Energy Office of Science by Stanford University. The SSRL Structural Molecular Biology Program is supported by the DOE Office of Biological and Environmental Research, and by the National Institutes of Health, National Institute of General Medical Sciences (including P41GM103393). The GM/CA CAT has been funded in whole or in part with Federal funds from National Cancer Institute (Y1-CO-1020) and National Institute of General Medical Sciences (Y1-GM-1104). Use of the Advanced Photon Source was supported by the US Department of Energy, Basic Energy Sciences, Office of Science, under contract no. DE-AC02-06CH11357. The content is solely the responsibility of the authors and does not necessarily represent the official views of NIGMS or the NIH. This is The Scripps Research Institute manuscript number 25075.

Author contributions

P.S.L., N.O., Y.K. and I.A.W. designed the research; P.S.L., W.Y. and Y.I. performed the research; P.S.L., R.L.S. and I.A.W. analysed data; Y.O., Y.K. and I.A.W. supervised the project; and P.S.L. and I.A.W. wrote the manuscript.

Additional information

Accession codes: Coordinates and structure factors have been deposited in the RCSB Protein Data Bank under accession codes 4O58 (F045–092–Vic1975/H3 complex), 4O5I (F045–092–Vic2011/H3 complex), 4O5L (apo F045–092 Fab) and 4O5N (apo Vic2011/H3 HA).

Supplementary Information accompanies this paper at http://www.nature.com/naturecommunications

Competing financial interests: The authors declare no competing financial interests.

Reprints and permission information is available online at http://npg.nature.com/reprintsandpermissions/

How to cite this article: Lee, P. S. *et al.* Receptor mimicry by antibody F045–092 facilitates universal binding to the H3 subtype of influenza virus. *Nat. Commun.* 5:3614 doi: 10.1038/ncomms4614 (2014).

OPEN

Nanogel-based pneumococcal surface protein A nasal vaccine induces microRNA-associated Th17 cell responses with neutralizing antibodies against *Streptococcus pneumoniae* in macaques

Y Fukuyama[1], Y Yuki[1,2], Y Katakai[3], N Harada[4], H Takahashi[5], S Takeda[5], M Mejima[1], S Joo[1], S Kurokawa[1], S Sawada[5], H Shibata[6], EJ Park[1], K Fujihashi[7], DE Briles[8], Y Yasutomi[6], H Tsukada[4], K Akiyoshi[5] and H Kiyono[1,2]

We previously established a nanosized nasal vaccine delivery system by using a cationic cholesteryl group-bearing pullulan nanogel (cCHP nanogel), which is a universal protein-based antigen-delivery vehicle for adjuvant-free nasal vaccination. In the present study, we examined the central nervous system safety and efficacy of nasal vaccination with our developed cCHP nanogel containing pneumococcal surface protein A (PspA-nanogel) against pneumococcal infection in nonhuman primates. When [^{18}F]-labeled PspA-nanogel was nasally administered to a rhesus macaque (*Macaca mulatta*), longer-term retention of PspA was noted in the nasal cavity when compared with administration of PspA alone. Of importance, no deposition of [^{18}F]-PspA was seen in the olfactory bulbs or brain. Nasal PspA-nanogel vaccination effectively induced PspA-specific serum IgG with protective activity and mucosal secretory IgA (SIgA) Ab responses in cynomolgus macaques (*Macaca fascicularis*). Nasal PspA-nanogel-induced immune responses were mediated through T-helper (Th) 2 and Th17 cytokine responses concomitantly with marked increases in the levels of miR-181a and miR-326 in the serum and respiratory tract tissues, respectively, of the macaques. These results demonstrate that nasal PspA-nanogel vaccination is a safe and effective strategy for the development of a nasal vaccine for the prevention of pneumonia in humans.

INTRODUCTION

Streptococcus pneumoniae is a major cause of bacterial infections throughout the world and is involved in the induction of a wide variety of infectious diseases, including otitis media, pneumonia, bacteremia, and meningitis in children and adults. This organism is usually a commensal bacterium in the upper respiratory tract of humans. Currently, four pneumococcal vaccines, 7-, 10- and 13-valent polysaccharide conjugate vaccines (PCV7, 10, 13) for children and a 23-valent pneumococcal polysaccharide vaccine (PPV23) for adults, have been developed for public use and are delivered by intramuscular injection.[1–3] However, as the conjugate vaccine does not protect against other capsular types, it provides little or no protection against total colonization with pneumococci.[4,5] The extensive carriage by other pneumococcal capsular types has led to strain replacement in disease with strains of non-conjugate vaccine capsular types.[6,7]

[1]Division of Mucosal Immunology, The Institute of Medical Science, The University of Tokyo, Minato-ku, Tokyo, Japan. [2]International Research and Development Center for Mucosal Vaccine, The Institute of Medical Science, The University of Tokyo, Minato-ku, Tokyo, Japan. [3]Corporation for Production and Research of Laboratory Primates, Tsukuba, Ibaraki, Japan. [4]PET Center, Central Research Laboratory, Hamamatsu Photonics K.K., Hamamatsu, Shizuoka, Japan. [5]Department of Polymer Chemistry, Kyoto University Graduate School of Engineering, Nishikyo-ku, Kyoto, Japan. [6]Tsukuba Primate Research Center, National Institute of Biomedical Innovation, Tsukuba, Ibaraki, Japan. [7]Departments of Pediatric Dentistry and Microbiology, The Immunobiology Vaccine Center, The University of Alabama at Birmingham, Birmingham, Alabama, USA and [8]Department of Microbiology, The University of Alabama at Birmingham, Birmingham, Alabama, USA. Correspondence: Y Yuki or H Kiyono (yukiy@ims.u-tokyo.ac.jp or kiyono@ims.u-tokyo.ac.jp)

Received 1 June 2014; accepted 2 January 2015; advance online publication 11 February 2015. doi:10.1038/mi.2015.5

The development of effective protein-based vaccines, which have the potential to provide better coverage for all strains, and to protect against colonization with all strains requires a thorough understanding of the roles and relative contributions to pathogenesis of the various putative virulence proteins. The pneumococcal surface protein A (PspA) is a well-known highly immunogenic surface protein of *S. pneumoniae* and is considered to be a promising vaccine candidate.[8,9] It is present on virtually all strains of pneumococci, and PspA-based vaccines against *S. pneumoniae* induce cross-reactive Abs in mice[10,11] and humans.[12] Moreover, PspA-specific mucosal and serum Abs responses are induced, and these responses are mediated by both Th1- and Th2-type cytokine production by $CD4^+$ T cells in infant mice via maternal immunization,[13] as well as in aged mice.[14] These findings indicate that PspA is a potent antigen for the development of effective pneumococcal vaccines not only in adults but also in children and the elderly.

S. pneumoniae commonly colonizes the nasal cavity, which can be protected by mucosal IgA.[15–17] Nasal vaccination induces effective mucosal immune responses in the respiratory tract, where initial bacterial and viral infections commonly occur; it could therefore be an effective immunization strategy for delivering protection from pneumococcal infection. However, most subunit type vaccines are poor immunogens for the induction of antigen-specific immune response in both systemic and mucosal immune compartments when nasally administered. Thus, the co-administration of biologically active mucosal adjuvants (e.g., cholera toxin and heat-labile toxin) or a better delivery system is needed to overcome the disadvantages of nasal antigen exposure. However, there are currently no safe nasal adjuvants or delivery systems, as evaluated by safety pharmacology studies, such as absorption, distribution, metabolism, and excretion in preclinical studies.

To overcome these concerns, we recently developed an effective vaccine delivery system with a self-assembled nanosized hydrogel (nanogel), which is composed of a cationic type of cholesteryl group-bearing pullulan (cCHP).[18] This cCHP nanogel efficiently delivers an antigen to epithelial cells in the nasal cavity, as well as to dendritic cells (DCs) under the basement membrane, and induces antigen-specific immune responses as an adjuvant-free vaccine.[19,20] Furthermore, a radioisotope counting assay showed that nasally administered cCHP nanogel carrying the [^{111}In]-labeled non-toxic subunit of botulinum neurotoxin does not accumulate in parts of the central nervous system (CNS) in mice.[19] In our separate study, we demonstrated that a nasally administered PspA-nanogel vaccine is safe and induces strong antigen-specific systemic and mucosal Ab immune responses, which can protect mice from invasive challenge with *S. pneumoniae*.[21]

MicroRNAs (miRNAs) have emerged as important regulators of many biological processes associated with the immune system, including the function of both innate and adaptive immune responses.[22–24] Accumulating evidence indicates that miRNA has an essential role in eliciting immune responses. For example, mice with T lymphocytes in which the endoribonuclease dicer, which is critical for miRNA biogenesis, has been conditionally knocked out show impaired thymic development and diminished Th-cell differentiation.[25,26] Dicer deficiency in B cells also prevents B-cell development.[27] These findings indicate the critical functions of miRNAs in the biology of the cells that constitute the immune system, such as in the development and differentiation of lymphocytes. Therefore, it is important to identify the miRNA biomarkers that engage in both mucosal and systemic antibody responses induced by nasal immunization with PspA-nanogel. Together, better understanding of the precise engagement of miRNAs in mediating humoral and protective immunity will be beneficial for the development of effective mucosal vaccines.

Before pursuing a clinical trial of a PspA-nanogel-based vaccine, we designed experiments to assess its safety for the CNS and its immunological efficacy, including immunologically relevant miRNA expression, and to demonstrate its safety and efficacy in nonhuman primates.

RESULTS

[^{18}F]-PspA-nanogel is retained for a long time in the nasal cavity but is not deposited in the olfactory bulbs or brain after nasal administration in macaques

We initially confirmed the physicochemical characterization of PspA-nanogel vaccine used in this study (**Supplementary Figure S1** online), and then investigated the retention of nasal PspA-nanogel in the nasal cavity and its accumulation in the olfactory bulbs and CNS in nonhuman primates by using three naive rhesus macaques. Because the results were nearly identical for the three macaques, we show the results for only one of the macaques in **Figure 1** (primate #1). The macaque's head was placed in the positron emission tomography (PET) scanner system and real-time imaging was performed for 6 h. To confirm the exact position of the cerebrum, we performed a magnetic resonance imaging (MRI) scan and then superimposed the PET images onto the MRI images. The real-time PET images clearly showed that nasally administered [^{18}F]-PspA-nanogel was effectively delivered to the nasal mucosa and retained in the nasal tissues for up to 6 h (**Figure 1a,c**). In contrast, most of the free form of [^{18}F]-PspA without a nanogel had disappeared from the nasal cavity by 3 h after nasal administration (**Figure 1a**). Furthermore, no deposition of [^{18}F]-PspA was detected in the cerebrum or olfactory bulbs of macaques, even 6 h after nasal administration (**Figure 1b**). These results show that PspA-nanogel is a CNS-safe and effective nasal vaccine delivery system in nonhuman primates.

Nasal vaccination with PspA-nanogel induces mucosal and systemic Ab responses in macaques

We next examined whether the nasal PspA-nanogel vaccine induced PspA-specific immune responses in cynomolgus macaques (primates #2-#9). One week after the final immunization, PspA-specific serum IgG Ab responses were significantly increased in macaques nasally immunized with 25 μg of PspA-nanogel when compared with macaques immunized with PspA alone or PBS only (**Figure 2a**). Examination of the longevity of PspA-nanogel-induced serum antigen-specific IgG

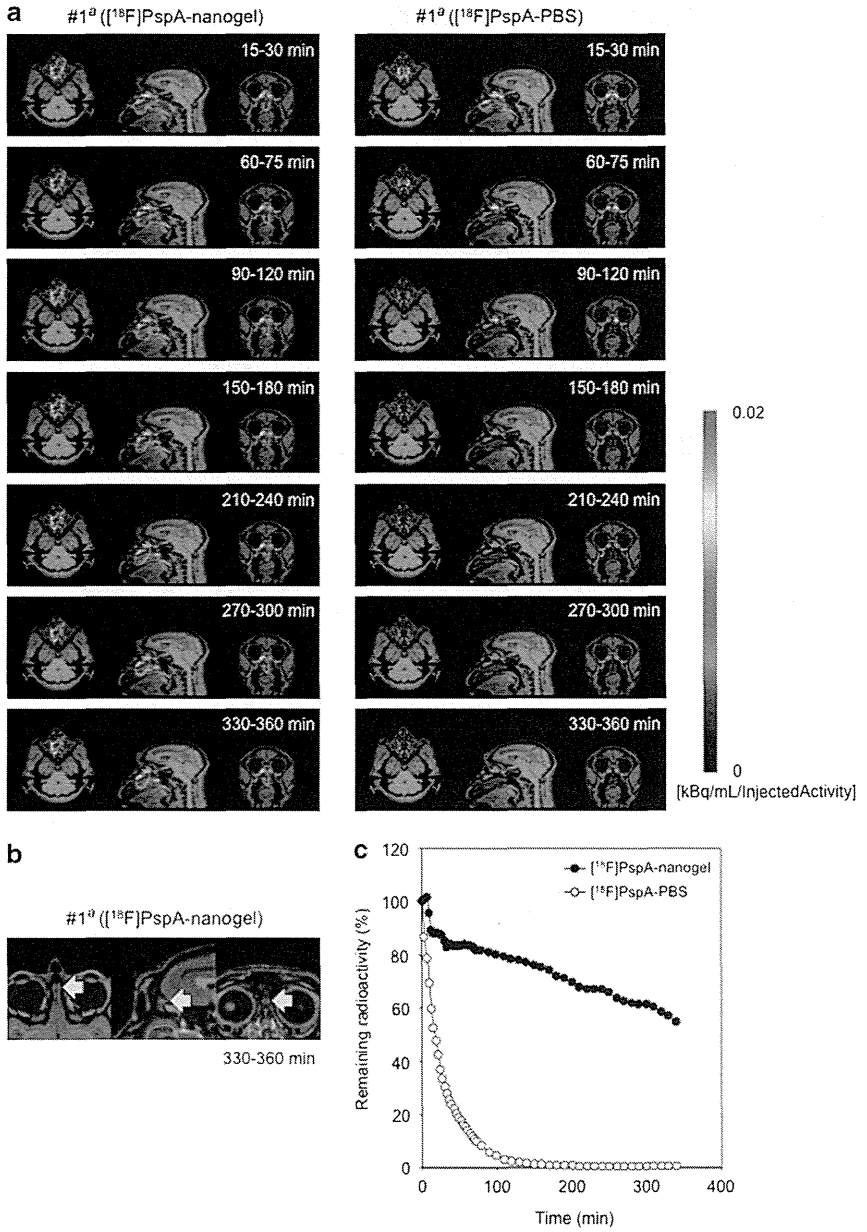

Figure 1 PET/MRI images (**a**,**b**) and TACs (**c**) for nasal administration of [^{18}F]-PspA-nanogel or [^{18}F]-PspA-PBS in a naive rhesus macaque. (**a**) After nasal administration of [^{18}F]-PspA-nanogel or [^{18}F]-PspA-PBS, the macaque's head was scanned for 6 h with a PET scanner. Real-time PET images overlaid on MRI images are shown for the indicated times post-administration. (**b**) To further check whether [^{18}F]-PspA accumulated in the CNS or olfactory bulbs (indicated by arrowheads), PET images taken at 6 h post-administration of [^{18}F]-PspA-nanogel were enlarged. (**c**) TACs for the nasal cavity for 6-h period after nasal administration of [^{18}F]-PspA-nanogel or [^{18}F]-PspA-PBS are presented. The data are expressed as percentages of the dose remaining after nasal administration. *a*: The same macaque was nasally administered of [^{18}F]-PspA-nanogel or [^{18}F]-PspA-PBS with a 1-week interval between administrations. CNS, central nervous system; MRI, magnetic resonance imaging; PET, positron emission tomography; TACs, time-activity curves.

Ab titers revealed that Ab levels gradually decreased over a period of 8 months in macaques nasally immunized with PspA-nanogel. Similarly, PspA-specific bronchoalveolar lavage fluid (BALF) IgG and nasal wash IgA Ab responses exhibited higher levels in macaques nasally immunized with PspA-nanogel when compared with macaques nasally immunized with PspA alone or PBS only (**Figure 2b,c**), and these Ab levels were also gradually decreased. In addition, PspA-specific BALF IgA Ab responses were slightly increased in two of the immunized macaques (#3 and #5) (**Figure 2c**).

When these macaques were given a dose of nasal booster of PspA-nanogel 9 months after the final immunization, the levels of PspA-specific serum and BALF IgG and nasal wash IgA Ab responses immediately recovered to those observed at 9 weeks

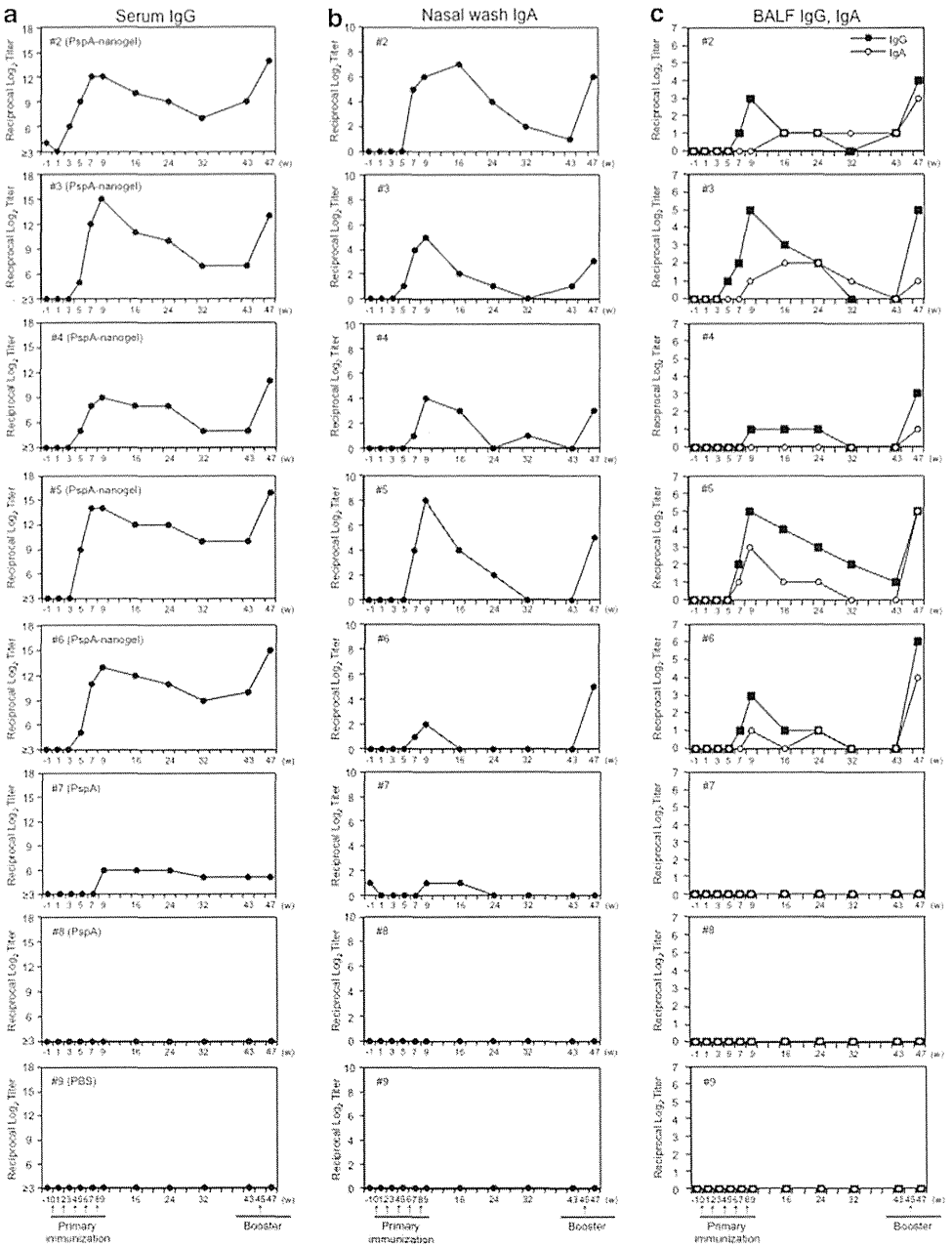

Figure 2 Nasal immunization with PspA-nanogel induced PspA-specific Ab responses in macaques. Each cynomolgus macaque was nasally immunized with PspA-nanogel (macaques #2-#6), PspA alone (#7 and #8), or PBS only (#9) at the times indicated with arrows. Serum, nasal wash, and BALF were collected, and the levels of PspA-specific serum IgG (**a**), nasal wash IgA (**b**), and BALF IgG and IgA (**c**) were determined by ELISA. BALF, bronchoalveolar lavage fluid.

after the initial PspA-nanogel immunization (**Figure 2a–c**). Of importance, a nasal booster induced higher levels of PspA-specific IgA Ab responses in BALF of two macaques (#5 and #6) than those observed after the primary immunization (**Figure 2c**).

These findings suggest that memory-type PspA-specific Ab responses are induced in nonhuman primates after nasal vaccination with PspA-nanogel. PspA-nanogel is therefore a promising nasal vaccine candidate that can induce long-lasting antigen-specific systemic and mucosal immunity and can elicit nasal booster activity in nonhuman primates.

Nasal immunization with PspA-nanogel induces neutralizing Abs against *S. pneumoniae* in macaques

To investigate whether the nasal PspA-nanogel vaccine induced neutralizing Abs, we examined whether PspA-specific serum Abs from macaques nasally immunized with PspA-nanogel would passively protect against pneumococcal infection. CBA/N mice were injected intraperitoneally with diluted pooled sera of macaques nasally immunized with PspA-nanogel, PspA alone, or PBS only. When all groups of mice were challenged with *S. pneumoniae* Xen10 or 3JYP2670 strain via the intravenous route, mice passively immunized with sera

from macaques nasally immunized with PspA-nanogel were fully protected for at least 2 weeks (**Figure 3a,b**). In contrast, mice that received sera from macaques given nasal PspA alone or PBS only died within 5 days post-challenge (**Figure 3a,b**). These results demonstrated that protective immunity with subtype cross-reactivity was induced by nasal PspA-nanogel vaccination.

Nasal immunization with PspA-nanogel induces Th2 and Th17 responses in macaques

As macaques nasally immunized with PspA-nanogel showed high IgG/IgA Ab responses, we next determined the levels of cytokine production in $CD4^+$ T cells isolated from blood of the macaques. The macaques nasally immunized with PspA-nanogel showed increased levels of IL-4 and IL-17 production by $CD4^+$ T cells when compared with macaques given PspA alone or PBS only (**Figure 4b,c**). However, essentially identical levels of IFN-γ were produced by $CD4^+$ T cells isolated from macaques nasally immunized with PspA-nanogel, PspA alone, or PBS only (**Figure 4a**). Furthermore, we showed that nasal immunization with PspA-nanogel induced PspA-specific IgG1 Ab responses, which is the hallmark of the Th2-type immune response (**Figure 4d**). These results indicated that the nasal PspA-nanogel vaccine could induce Th2 and Th17 cytokine responses.

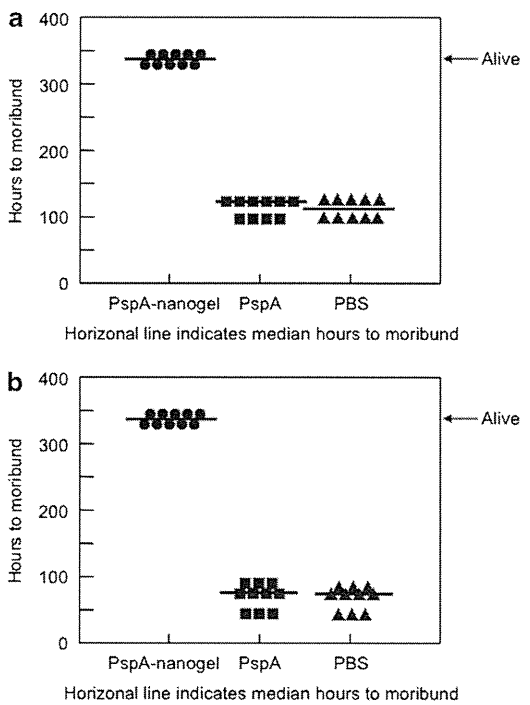

Figure 3 Neutralizing Abs induced by nasal immunization with PspA-nanogel. Serum from each of the macaques was collected 1 week after the final primary nasal immunization with PspA-nanogel, PspA alone, or PBS only. CBA/N mice (10 mice per group) were passively transferred with 100 μl of diluted (1:20) pooled sera via i.p. route. Four hours later, mice were injected i.v. with 1.5×10^4 c.f.u. *S. pneumoniae* Xen 10 (**a**) or 1×10^3 c.f.u. *S. pneumoniae* 3JYP2670 strain (**b**). The mice were monitored daily for mortality. Each line represents the median survival time. c.f.u., colony-forming unit; i.p., intraperitoneal; i.v., intravenous.

Nasal immunization with PspA-nanogel increases the expression levels of miRNAs in serum and respiratory tract tissues in macaques

To examine the roles of miRNA in the induction of PspA-specific immunity, we performed miRNA microarray analysis to identify immunologically associated differences in serum miRNA profiles between pre-immunized and post-boosted macaques (data not shown). We selected some immunologically relevant miRNAs, namely miR-181a, miR-326, miR-155, miR-17, miR-18a, miR-20a, and miR-92a, the levels of which were upregulated in post-booster serum samples compared with pre-immunized serum samples. To further confirm whether these immunologically relevant miRNAs were upregulated or downregulated in post-booster serum samples compared with pre-immunized or pre-booster serum samples, we performed quantitative RT–PCR of them. Expression levels of miR-326, Th17-cell differentiation-related miRNA, and miR-181a, T-cell and B-cell differentiation-related miRNA, were significantly increased in the sera of macaques given a nasal booster dose of PspA-nanogel when compared with control macaques as pre-immunization (**Figure 5a**). The levels of the two miRNAs were also shown significantly higher in the respiratory tract tissues, including nasal tissues and lungs, of macaques given a booster dose of PspA-nanogel than the levels in the corresponding tissues of control macaques given PspA alone or PBS only that was set at 1 (**Figure 5b,c**). Furthermore, we analyzed the expression level of Ets-1, which is a known negative regulator of Th17 cells and is the functional target of miR-326. We detected a significant decrease in the expression level of Ets-1 mRNA in the lungs of macaques given a booster dose of PspA-nanogel compared with those of control macaques given PspA alone or PBS only (**Figure 5c**). These results suggest that these miRNAs have important roles in T-cell and B-cell differentiation and in Th17 cytokine responses after nasal immunization with PspA-nanogel in macaques.

DISCUSSION

By using a nonhuman primate system, we demonstrated that the nasal PspA-nanogel vaccine did not accumulate in the CNS and effectively induced both mucosal and systemic immunity associated with protection against pneumococcal infection. To our knowledge, this study is the first to report the safety and effectiveness of a nasal PspA vaccine in macaques; therefore, our results provide a concrete rationale for testing our nanogel-based PspA vaccine in humans.

The nanogel itself is non-immunogenic material, and a cancer-specific protein (e.g., Her 2) complexed with a neutral CHP nanogel produced by means of good manufacturing practices (GMP) has been used as an injectable cancer vaccine in clinical research.[28] In our previous study, nasal immunization with CHP-nanogel containing PspA induces effective antigen-specific immune responses in mice[21] but not in macaques (data not shown); therefore, in the present study, we developed a cCHP nanogel containing 20 amino groups per 100 glucose units to improve antigen delivery to the nasal

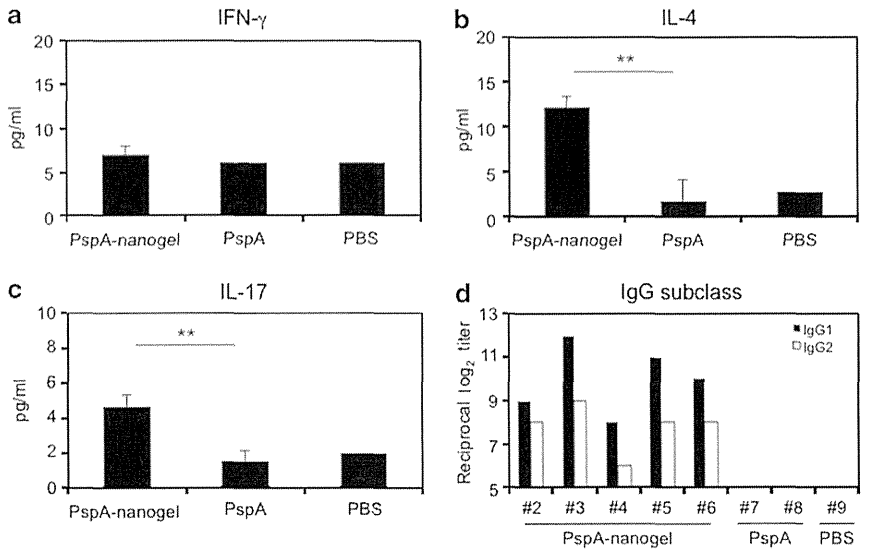

Figure 4 PspA-nanogel immunization produced $CD4^+$ Th2- and Th17-type cytokine responses. $CD4^+$ T cells were separated from the PBMCs 1 week after the booster. Purified $CD4^+$ T cells were cultured with irradiated APCs and 5 μg ml^{-1} of PspA with anti-CD28 and CD49d antibodies for 5 days. The levels of the cytokines, IFN-γ (**a**), IL-4 (**b**), and IL-17A (**c**) in the supernatants were measured. This experiment was repeated in triplicate. Values are shown as the means ± s.d. in each experimental group. $^{**}P < 0.01$ compared between PspA-nanogel and PspA/PBS groups. (**d**) Serum from macaques was collected 1 week after the final primary nasal immunization with PspA-nanogel (#2-#6), PspA alone (#7, #8), or PBS only (#9). Expression levels of PspA-specific serum IgG subclass Abs were determined by using ELISA. APCs, antigen-presenting cells; IFN, interferon; IL, interleukin; PBMC, peripheral blood mononuclear cells.

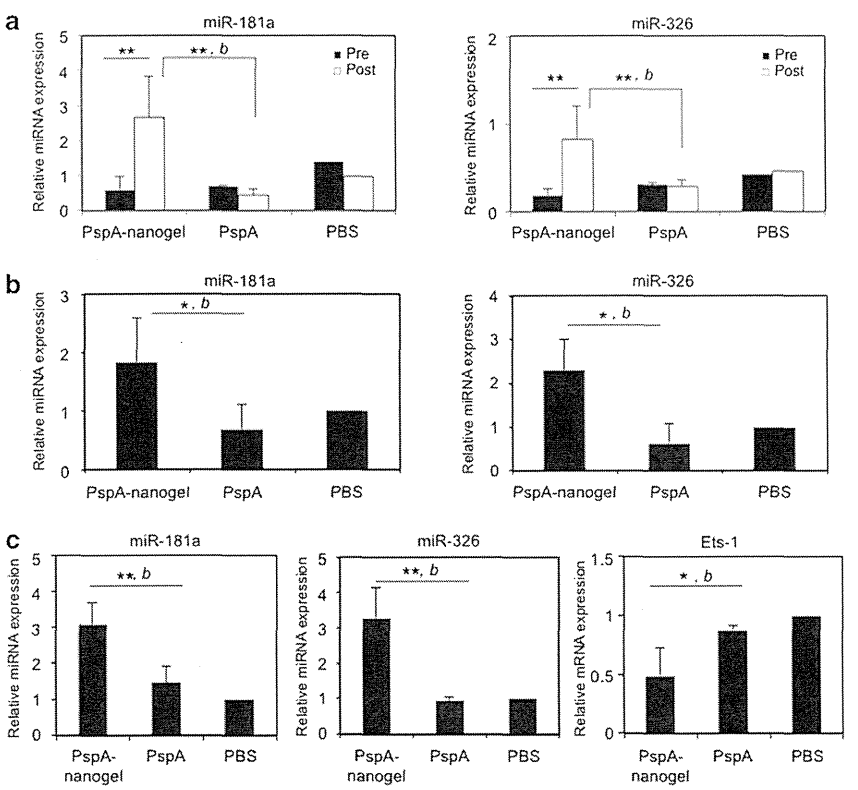

Figure 5 MiRNA expression levels in sera (**a**), nasal tissues (**b**), and lung tissues (**c**) of macaques nasally immunized with PspA-nanogel, PspA alone, or PBS only. Expression levels of the indicated miRNA and Ets-1 mRNA were analyzed by quantitative RT–PCR and normalized to the levels of miR-16 and β-actin, respectively. Values are shown as the means ± s.d. in each experimental group. $^{*}P < 0.05$, $^{**}P < 0.01$ when compared between pre-immunization and post-booster groups. *b*, Compared between PspA-nanogel and PspA/PBS groups in post-booster macaques. MiRNA, microRNA; Pre, pre-immunized serum; Post, post-booster serum.

epithelium layer of macaques. We confirmed the perfect complex formation and the size of PspA-nanogel complex using fluorescence response energy transfer (FRET) analysis and dynamic light scattering (DLS): the cCHP nanogel spontaneously formed nanoparticles after the incorporation of PspA (**Supplementary Figure S1a,b**).[18,19] In addition, consistent with its positive zeta-potential (**Supplementary Figure S1b**), *in vivo* PET and MRI imaging in macaques clearly showed that nasally administered cCHP nanogel carrying [^{18}F]-labeled PspA was more effectively delivered to and continuously retained at the nasal mucosa of macaques when compared with nasally delivered [^{18}F]-PspA alone. These results indicated that the new cationic group-modified cCHP nanogel would be able to efficiently deliver the vaccine antigen to the anionic nasal epithelium following nasal administration in macaques. Indeed, our previous mouse model studies have shown that the nanogel–antigen complex is retained and taken up into the epithelium by endocytosis, where the antigen is released from the nanogel in the epithelium by strong chaperone-like activity. The antigen is then released from the nasal epithelium by exocytosis and subsequently taken up effectively by DCs.[19,21]

Recent studies of nasal vaccines have raised concerns about the deposition and accumulation of candidate vaccine antigens or co-administered mucosal adjuvants in the CNS through direct transport from the nasal cavity to the cerebrum via the olfactory pathways.[29,30] It has also been reported that many peptides and proteins bypass the blood–brain and blood–cerebrospinal fluid barriers to reach the CNS following nasal administration in humans.[31] In this study, we showed that there was no deposition or accumulation of [^{18}F]-PspA in the CNS over a period of up to 6 h after nasal administration of [^{18}F]-PspA-nanogel in macaques. As we validated the detection limit of our PET system for [^{18}F]-protein by direct tissue counting in our previous study,[32] [^{18}F] radioactivity in this study was <0.05 SUV in the cerebrum and olfactory bulbs of the macaques. Therefore, our current results demonstrated that the cCHP delivered nasal PspA vaccine did not reach the CNS of macaques, even though the olfactory epithelium in the nasal cavity is connected to the CNS,[31] thereby confirming the safety of the vaccine in higher mammals.

The mucosal immune system consists of both inductive and effector sites and has a key role in the induction and regulation of dynamic immune responses, including the Th2-type-cell-dependent SIgA response, the mucosal cytotoxic T-cell response, and the Th17-cell-mediated immune regulatory response.[33] In general, IgA in mucosal tissue is thought to have an important role in protection against respiratory pathogens including *S. pneumoniae*.[15–17] In this study, we showed that the PspA-nanogel vaccine also induced mucosal antigen-specific mucosal IgA and systemic IgG Ab responses in the macaques. Especially, serum and BALF IgG, the main isotype of antibody in the lower respiratory compartment, have key roles in survival against lethal challenge with *S. pneumoniae*.[34] Importantly, the macaque IgG antibodies to PspA, which are supported by CD4$^+$ Th2-type cytokine IL-4, possessed protective activity against *S. pneumoniae*. When mice were systemically challenged with *S. pneumoniae* Xen10 or 3JYP2670 after mice passively immunized with macaques' sera containing PspA-specific Abs, they showed complete protection. Our findings indicate that this protection is clearly due to antibody-mediated immunity to PspA. These results are consistent with those of a previous study in mice showing that nasal vaccination induces functional CD4$^+$ Th2-type cytokine-mediated IgG Ab responses, which are sufficient to provide appropriate protection in the absence of Th1-type cytokine responses.[16] In addition, induction of the BALF IgG responses is essential, as antigen-specific IgG is known to exert protection at the alveolar level following to promote phagocytosis and prevents local dissemination of the pneumococcus and its passage into the blood.[34] These results demonstrated that the nasal PspA-nanogel vaccine effectively induced PspA-specific serum IgG with protective activity in addition to SIgA Ab immune responses in nonhuman primates.

Recent studies have shown that specific miRNAs are involved in T-cell and B-cell development, differentiation, and regulatory functions.[24,35] Especially, miR-181a is highly expressed in mature T cells and has an important effect on the positive and negative selection process by controlling the strength of TCR signaling during thymic development of T cells for subsequent Th1 and Th2 differentiation, indicating that miR-181a modulates T-cell development.[36] In this study, the expression levels of miR-181a in the serum and respiratory tract tissues, including nasal tissues and lungs, were significantly higher in macaques nasally immunized with PspA-nanogel than in those given PspA alone or PBS only, indicating that miRNAs are implicated in adaptive immunity by controlling the activation of T cells after nasal immunization with PspA-nanogel in nonhuman primates. Furthermore, we showed that the levels of miR-155, which is required for the production of high-affinity IgG1 Abs, were increased in PspA-nanogel-immunized macaques (**Supplementary Figure S2a–c**).[37] These results indicated that PspA-nanogel-induced Th2 cytokine response was mediated through the increased expression of miR-155.

MiR-181a is also highly expressed in B cells and within bone marrow cells and germinal center B cells, where it promotes the differentiation of hematopoietic stem cells into B cells.[24,38] To explore the roles of other miRNAs that are also highly expressed in germinal center B cells and are essential for adult B-cell development, we examined the expression of the miR-17-92 cluster.[39,40] The miR-17-92 cluster regulates follicular helper T cell (Tfh cell) differentiation by controlling the migration of CD4$^+$ T cells into B-cell follicles,[41] suggesting that these miRNAs have an important role in the production of antigen-specific SIgA Ab. We found here that not only miR-181a expression but also miR-17-92 cluster expression was markedly increased in the nasal tissues of nasally PspA-nanogel-immunized macaques (**Supplementary Figure S3**). Detection of these mucosal IgA-associated miRNAs in the nasal tissues of nasally PspA-nanogel-immunized macaques

indicates that they contribute substantially to the production of mucosal IgA.

It is well known that IL-17-mediated $CD4^+$ T cells are important for the generation of resistance to mucosal colonization by respiratory pathogens including *S. pneumoniae* in humans and mice.[42,43] Trzcinski *et al.*[44] demonstrated that antigen-specific $CD4^+$ T-cell immunity is sufficient to protect against nasopharyngeal colonization by *S. pneumoniae* in mice. Studies in mice indicated that pulmonary Th17 responses are associated with migration of B cells into airways and with the promotion of polymeric Ig receptor (pIgR) expression by airway epithelial cells.[45] In addition, Th17 cells are a crucial subset of Th cells responsible for inducing the switch of germinal center B cells toward T-cell-dependent IgA production.[46] Furthermore, IL-17-secreting memory Th17 cells increased by human pneumococcal carriage have been reported to enhance innate cellular immunity against pneumococcal challenge.[47] Therefore, it is important to determine whether antigen-specific $CD4^+$ Th17 responses are induced by nasal immunization with PspA-nanogel in nonhuman primates. Recent studies have shown that miR-326-mediated Th17 upregulation might provide the host with a potentiating effect to recruit functional immune cells to local effector sites in response to pathogen attack.[48] We found here that nasal immunization with PspA-nanogel in macaques prompted the generation of IL-17-producing cells in the peripheral blood $CD4^+$ T cells. Furthermore, our miRNA analysis showed that expression levels of Th17-associated miR-326 in the serum, nasal tissues, and lungs were significantly increased and that the expression level of Ets-1 mRNA, a negative regulator of Th17 differentiation, was decreased in the lungs of the PspA-nanogel-vaccinated macaques. Therefore, our finding that miR-326-associated IL-17-secreting $CD4^+$ T cells were generated after nasal vaccination with PspA-nanogel suggests that it would be useful for the development of safe and efficacious nasal vaccines against pneumonia and that serum miR-326 could be used as a biomarker to evaluate vaccine efficacy.

In summary, we demonstrated for the first time that a nasal PspA-nanogel vaccine induced both humoral and cellular immune responses in macaques. These results were supported by increased expression levels of miR-181a and miR-326, which are candidate miRNA biomarkers for induction of mucosal immunity. In addition, a [^{18}F]-PspA PET study showed long-term retention of PspA in the nasal cavity and no deposition of PspA in the CNS of the macaques. Taken together, these findings demonstrate the efficacy and safety of nasal PspA-nanogel vaccine in nonhuman primates. We conclude that the nasal PspA-nanogel vaccine should now be studied in humans for its possible use as an adjuvant-free nasal vaccine.

METHODS

Animals. Eight female naive cynomolgus macaques (*Macaca fascicularis*, 5 years old, ~3 kg) were used for the immunization study and were maintained at the Tsukuba Primate Research Center for Medical Science at the National Institute of Biomedical Innovation (NIBIO, Ibaraki, Japan). In a separate experiment, one naive male rhesus macaque (*M. mulatta*, 5–6 years old, ~5 kg) was used for the PET imaging study, which was conducted at PET Center of Hamamatsu Photonics K.K. To assay antibody protection against *S. pneumoniae*, female CBA/N mice (6 weeks old) were purchased from Japan SLC (Shizuoka, Japan). All experiments were performed in accordance with the Guidelines for Use and Care of Experimental Animals, and the protocol was approved by the Animal Committee of NIBIO, Hamamatsu Photonics K.K., and The University of Tokyo.

Recombinant PspA. Recombinant PspA of *S. pneumoniae* Rx1, which belongs to PspA family 1 and clade 2, was prepared as described previously, with slight modification.[10] In brief, the plasmid encoding PspA/Rx1 (GenBank accession no. M74122; amino acids 1 through 302, pUAB055) was used to transform *E. coli* BL21 (DE3) cells. To construct pUAB055, a 909-bp fragment of PspA from a pneumococcal strain Rx1 was cloned into the pET20b vector (Novagen, Darmstadt, Germany) between the *Nco*I and *Xho*I sites. Recombinant PspA/Rx1 contains the first 302 amino acids of mature PspA plus six poly-histidines added through protein fusion at the C-terminal end. The sonicated cell supernatant was loaded onto a DEAE-Sepharose column (BD Healthcare, Piscataway, NJ) and a nickel affinity column (Qiagen, Valencia, CA), followed by gel filtration on a Sephadex G-100 column (BD Healthcare).

Preparation of recombinant PspA–nanogel complex. The cCHP nanogel (~40 nm size) generated from cationic type of cholesteryl group-bearing pullulan was used for all experiments. This cCHP nanogel contained 20 amino groups per 100 glucose units. The PspA-cCHP nanogel complex for each immunization was prepared by mixing 25 μg of PspA with cCHP at a 1:5 molecular ratio (59.45 μl per macaque) and incubating for 1 h at 46 °C. FRET was determined with an FP-6500 fluorescence spectrometer (JASCO, Tokyo, Japan) with FITC-conjugated PspA and TRITC-conjugated cCHP nanogel.[18,19] The hydrodynamic radius was assessed by means of DLS and the zeta-potential of cCHP carrying or not carrying, PspA was determined with a Zetasizer Nano ZS instrument (Malvern Instruments, Worcestershire, UK).[18,19]

Nasal immunization and sample collection. Cynomolgus macaques were nasally immunized five times at 2-week intervals with PspA-nanogel under ketamine anesthesia. For the control group, macaques were nasally administered with 25 μg of PspA alone, or PBS only. Eight months after the final immunization, the macaques were nasally boosted with the same amount of PspA-nanogel, PspA alone or PBS only. Serum, nasal wash, and BALF were collected before primary immunization, 1 week after each immunization, 2, 4, 6, and 8 months after the final immunization, and 2 weeks after receipt of the booster.

PspA-specific ELISA. The antigen-specific Ab responses were analyzed by ELISA as described previously.[21] In brief, 96-well plates were coated with 1 $\mu g\,ml^{-1}$ PspA in PBS overnight at 4 °C. After blocking with 1 % BSA in PBS-Tween, twofold serial dilutions of samples were added and incubated for 2 h at room temperature (RT). After washing of the samples, horseradish peroxidise (HRP)-conjugated goat anti-monkey IgG (Nordic Immunological Laboratory, Tilburg, The Netherlands) or HRP-conjugated goat anti-monkey IgA (Cortex Biochem, San Leandro, CA) diluted 1:1,000 was added and incubated for 2 h at room temperature. For subclass analysis, sheep anti-human IgG1 and IgG2 (Binding Site, Birmingham, UK) and HRP-conjugated donkey anti-sheep IgG (Rockland, Limerick, PA) were used for detection. The reaction was developed with the use of TMB Microwell Peroxidase Substrate System (XPL, Gaithersburg, MD). End-point titers were expressed as the reciprocal $\log_2$ of the last dilution that gave an OD_{450} of 0.1 greater than the negative control.

Passive protection of mice with macaques' serum samples. Pooled serum samples from macaques nasally immunized with PspA-

nanogel, PspA alone, or PBS only were diluted with PBS (1:20) and injected into CBA/N mice via the intraperitoneal route (100 µl per mouse). Four hours later, all groups of mice were challenged with 1.5×10^4 CFU *S. pneumoniae* Xen 10 ($LD_{50} = 2 \times 10^2$ CFU for CBA/N mice) or 1×10^3 CFU *S. pneumoniae* 3JYP2670 strain ($LD_{50} = 7 \times 10^2$ CFU for CBA/N mice) via the intravenous route and observed daily for death for 2 weeks. Information about *S. pneumoniae* strains is available in **Supplementary Materials**.

PspA-specific CD4$^+$ T-cell responses. One week after the macaques had received the booster, lymphocytes were isolated from the peripheral blood by using Ficoll-Paque PLUS (GE Healthcare, Little Chalfont, UK). We could not separate the lymphocytes from two macaques (#3 and #6). After washing of the samples, CD4$^+$ T cells were purified by using CD4 microbeads and magnetic cell sorting (AutoMACS; Miltenyi Biotec, Auburn, CA). The cells remaining after the removal of CD4$^+$ and CD8$^+$ T cells (by using CD8 microbeads) were used as antigen-presenting cells after irradiation at 3,000 rad. Purified CD4$^+$ T cells (1×10^5 cells/well) and antigen-presenting cells (0.5×10^5 cells/well) were resuspended in RPMI 1640 (Nacalai Tesque, Kyoto, Japan) supplemented with 10 % FCS and penicillin-streptomycin (Gibco, Carlsbad, CA), and were cultured in 24-well plates for 5 days in the presence of 5 µg ml^{-1} PspA with anti-CD28 (clone CD28.2) and CD49d (clone 9F10) antibodies (0.5 µg ml^{-1} each; eBioscience, San Diego, CA) at 37 °C in 5% CO_2. Supernatants were then collected. The concentrations of the cytokines, IFN-γ, IL-4, and IL-17 in the supernatants were measured with a Monkey Singleplex Bead Kit (Invitrogen, Carlsbad, CA) and Bio-Plex 200 (Bio-Rad, Hercules, CA).

Synthesis of [^{18}F]-PspA. Purified PspA was radiolabeled by conjugation with *N*-succinimidyl-4-[^{18}F]fluorobenzoate ([^{18}F]SFB), which reacts with free amino groups, including the N-terminal and ε-Lys amino groups in the protein, as described previously.[19,32] The product was purified by gel-permeation chromatography (Superose 12, PBS, 1 ml min^{-1}), and the radioactive peak that eluted at 12.7 min was collected. The 615 MBq [^{18}F]-PspA was obtained at 150 min from the end of bombardment. The radiochemical purity and the decay-corrected radiochemical yield were 100 and 2.95%, respectively. The specific activity was 1,798 to 4,045 MBq mg^{-1} protein.

PET/MRI imaging in rhesus macaques. Because the half-life of [^{18}F] is only 110 min, we used the same naive macaque for nasal [^{18}F]-PspA-nanogel or [^{18}F]-PspA-PBS administration with a 1-week interval between administrations. After nasal administration of 50 MBq per 700 µl of [^{18}F]-PspA-nanogel or [^{18}F]-PspA-PBS (350 µl in each nostril), the macaque's head was tilted back for 10 min and then scanned in an upright position. PET scans were conducted for 345 min with frames of 25 × 3 min, followed by 27 × 10 min, with the use of a high-resolution animal PET scanner (SHR-7700; Hamamatsu Photonics, Shizuoka, Japan). MRI images were recorded with Signa Excite HDxt (3T; GE Healthcare) to identify the cerebrum regions.

Image data analysis. PET data were analyzed by means of the PMOD software package (PMOD Technologies, Zurich, Switzerland). Each PET image was superimposed on the corresponding MRI data to identify the volume of interest. Time-activity curves (TACs) of PET/MRI images were expressed as % remaining dose.

MiRNA expression levels in serum and respiratory tract tissues. Serum samples were collected before primary immunization and after booster with PspA-nanogel, PspA alone, or PBS only. The respiratory tract tissues, which included nasal epithelial and lung samples, were collected after booster immunization with PspA-nanogel, PspA alone, or PBS only. Total RNAs were isolated from serum by using TRIzol LS reagent, and from nasal tissue or lung by using TRIzol reagent (Invitrogen) following the manufacturer's protocol. All the miRNAs in the sample were polyadenylated by using poly(A) polymerase and ATP (Invitrogen). Following polyadenylation, SuperScript III RT and a specially designed Universal RT Primer (Invitrogen) were used to synthesize cDNA from the tailed miRNA population. Each of the first-strand cDNAs was analyzed by quantitative RT-PCR with Fast SYBR Green Master Mix and Step One Plus Real-Time PCR System (Applied Biosystems, Carlsbad, CA). The expression levels were normalized to miR-16, which is a commonly used internal control for miRNA expression.[49,50]

Analysis of Ets-1 expression. After total RNAs were isolated from lung tissue, cDNA was synthesized by using PrimeScript RT Master Mix (Takara, Shiga, Japan) following the manufacturer's protocol. The cDNA was analyzed by quantitative RT–PCR with Fast SYBR Green Master Mix and Step One Plus Real-Time PCR System (Applied Biosystems). The PCR primers were used as follows: Ets-1: F, 5′-TGG AGTCAACCCAGCCTATC-3′ and R, 5′-TCTGCAAGGTGTCTGTC TGG-3′; β-actin: F, 5′-TGACGTGGACATCCGCAAAG-3′ and R, 5′-CTGGAAGGTGGACAGCGAGG-3′. The expression levels were normalized to that of β-actin.

Statistical analysis. The results are presented as means ± s.d. Student's *t*-test was used for comparisons among groups. The *P* values <0.05 or <0.01 were considered to indicate statistical significance.

SUPPLEMENTARY MATERIAL is linked to the online version of the paper at http://www.nature.com/mi

ACKNOWLEDGMENTS

This work was supported by the Ministry of Health, Labour, and Welfare of Japan (Y. Y.), Global Center of Excellence Program "Center of Education and Research for the Advanced Genome—Based Medicine—For personalized medicine, the control of worldwide infectious diseases—"MEXT" Japan (Y.F. and H.K.), the Ministry of Education, Culture, Sports, Science, and Technology of Japan (Grant-in-Aid for Scientific Research S [23229004], H.K.), and the Core Research for Evolutional Science and Technology Program of the Japan Science and Technology Agency (H.K.). We are grateful to Drs. Natsumi Takeyama, Koji Kashima, and Tatsuhiko Azegami and Mr. Yuji Suzuki for their useful discussions and technical support.

DISCLOSURE

The authors declare no conflict of interest.

REFERENCES

1. Jackson, L.A. & Janoff, E.N. Pneumococcal vaccination of elderly adults: new paradigms for protection. *Clin. Infect. Dis.* **47**, 1328–1338 (2008).
2. Nuorti, J.P. & Whitney, C.G. Prevention of pneumococcal disease among infants and children - use of 13-valent pneumococcal conjugate vaccine and 23-valent pneumococcal polysaccharide vaccine - recommendations of the Advisory Committee on Immunization Practices (ACIP). *MMWR Recomm. Rep.* **59**, 1–18 (2010).
3. Oosterhuis-Kafeja, F., Beutels, P. & Van Damme, P. Immunogenicity, efficacy, safety and effectiveness of pneumococcal conjugate vaccines (1998-2006). *Vaccine* **25**, 2194–2212 (2007).
4. Dagan, R. *et al.* Reduction of nasopharyngeal carriage of Streptococcus pneumoniae after administration of a 9-valent pneumococcal conjugate vaccine to toddlers attending day care centers. *J. Infect. Dis.* **185**, 927–936 (2002).
5. Dagan, R. *et al.* Comparative immunogenicity and efficacy of 13-valent and 7-valent pneumococcal conjugate vaccines in reducing nasopharyngeal colonization: a randomized double-blind trial. *Clin. Infect. Dis.* **57**, 952–962 (2013).
6. Croney, C.M., Coats, M.T., Nahm, M.H., Briles, D.E. & Crain, M.J. PspA family distribution, unlike capsular serotype, remains unaltered following introduction of the heptavalent pneumococcal conjugate vaccine. *Clin. Vaccine Immunol.* **19**, 891–896 (2012).
7. Pilishvili, T. *et al.* Sustained reductions in invasive pneumococcal disease in the era of conjugate vaccine. *J. Infect. Dis.* **201**, 32–41 (2010).

8. Berry, A.M., Yother, J., Briles, D.E., Hansman, D. & Paton, J.C. Reduced virulence of a defined pneumolysin-negative mutant of *Streptococcus pneumoniae*. *Infect. Immun.* **57**, 2037–2042 (1989).
9. McDaniel, L.S. *et al.* Use of insertional inactivation to facilitate studies of biological properties of pneumococcal surface protein A (PspA). *J. Exp. Med.* **165**, 381–394 (1987).
10. Briles, D.E. *et al.* Intranasal immunization of mice with a mixture of the pneumococcal proteins PsaA and PspA is highly protective against nasopharyngeal carriage of *Streptococcus pneumoniae*. *Infect. Immun.* **68**, 796–800 (2000).
11. Nguyen, C.T., Kim, S.Y., Kim, M.S., Lee, S.E. & Rhee, J.H. Intranasal immunization with recombinant PspA fused with a flagellin enhances cross-protective immunity against *Streptococcus pneumoniae* infection in mice. *Vaccine* **29**, 5731–5739 (2011).
12. McCool, T.L., Cate, T.R., Moy, G. & Weiser, J.N. The immune response to pneumococcal proteins during experimental human carriage. *J. Exp. Med.* **195**, 359–365 (2002).
13. Kono, M., Hotomi, M., Hollingshead, S.K., Briles, D.E. & Yamanaka, N. Maternal immunization with pneumococcal surface protein A protects against pneumococcal infections among derived offspring. *PLoS One* **6**, e27102 (2011).
14. Fukuyama, Y. *et al.* A combination of Flt3 ligand cDNA and CpG oligodeoxynucleotide as nasal adjuvant elicits protective secretory-IgA immunity to *Streptococcus pneumoniae* in aged mice. *J. Immunol.* **186**, 2454–2461 (2011).
15. Ferreira, D.M. *et al.* Characterization of protective mucosal and systemic immune responses elicited by pneumococcal surface protein PspA and PspC nasal vaccines against a respiratory pneumococcal challenge in mice. *Clin. Vaccine Immunol.* **16**, 636–645 (2009).
16. Fukuyama, Y. *et al.* Secretory-IgA antibodies play an important role in the immunity to *Streptococcus pneumoniae*. *J. Immunol.* **185**, 1755–1762 (2010).
17. Janoff, E.N. *et al.* Killing of *Streptococcus pneumoniae* by capsular polysaccharide-specific polymeric IgA, complement, and phagocytes. *J. Clin. Invest.* **104**, 1139–1147 (1999).
18. Ayame, H., Morimoto, N. & Akiyoshi, K. Self-assembled cationic nanogels for intracellular protein delivery. *Bioconjug. Chem.* **19**, 882–890 (2008).
19. Nochi, T. *et al.* Nanogel antigenic protein-delivery system for adjuvant-free intranasal vaccines. *Nat. Mater.* **9**, 572–578 (2010).
20. Yuki, Y. *et al.* Nanogel-based antigen-delivery system for nasal vaccines. *Biotechnol. Genet. Eng. Rev.* **29**, 61–72 (2013).
21. Kong, I.G. *et al.* Nanogel-based PspA intranasal vaccine prevents invasive disease and nasal colonization by *Streptococcus pneumoniae*. *Infect. Immun.* **81**, 1625–1634 (2013).
22. Baltimore, D., Boldin, M.P., O'Connell, R.M., Rao, D.S. & Taganov, K.D. MicroRNAs: new regulators of immune cell development and function. *Nat. Immunol.* **9**, 839–845 (2008).
23. O'Connell, R.M., Rao, D.S., Chaudhuri, A.A. & Baltimore, D. Physiological and pathological roles for microRNAs in the immune system. *Nat. Rev. Immunol.* **10**, 111–122 (2010).
24. Zhu, S., Pan, W. & Qian, Y. MicroRNA in immunity and autoimmunity. *J. Mol. Med.* **91**, 1039–1050 (2013).
25. Cobb, B.S. *et al.* T cell lineage choice and differentiation in the absence of the RNase III enzyme Dicer. *J. Exp. Med.* **201**, 1367–1373 (2005).
26. Muljo, S.A. *et al.* Aberrant T cell differentiation in the absence of Dicer. *J. Exp. Med.* **202**, 261–269 (2005).
27. Koralov, S.B. *et al.* Dicer ablation affects antibody diversity and cell survival in the B lymphocyte lineage. *Cell* **132**, 860–874 (2008).
28. Kitano, S. *et al.* HER2-specific T-cell immune responses in patients vaccinated with truncated HER2 protein complexed with nanogels of cholesteryl pullulan. *Clin. Cancer Res.* **12**, 7397–7405 (2006).
29. van Ginkel, F.W., Jackson, R.J., Yuki, Y. & McGhee, J.R. Cutting edge: the mucosal adjuvant cholera toxin redirects vaccine proteins into olfactory tissues. *J. Immunol.* **165**, 4778–4782 (2000).
30. Yuki, Y. & Kiyono, H. Mucosal vaccines: novel advances in technology and delivery. *Expert Rev. Vaccines* **8**, 1083–1097 (2009).
31. Illum, L. Is nose-to-brain transport of drugs in man a reality? *J. Pharm. Pharmacol.* **56**, 3–17 (2004).
32. Yuki, Y. *et al.* In vivo molecular imaging analysis of a nasal vaccine that induces protective immunity against botulism in nonhuman primates. *J. Immunol.* **185**, 5436–5443 (2010).
33. Fukuyama, Y. *et al.* Novel vaccine development strategies for inducing mucosal immunity. *Expert Rev. Vaccines* **11**, 367–379 (2012).
34. Twigg, H.L. 3rd Humoral immune defense (antibodies): recent advances. *Proc. Am. Thorac. Soc.* **2**, 417–421 (2005).
35. Baumjohann, D. & Ansel, K.M. MicroRNA-mediated regulation of T helper cell differentiation and plasticity. *Nat. Rev. Immunol.* **13**, 666–678 (2013).
36. Li, Q.J. *et al.* miR-181a is an intrinsic modulator of T cell sensitivity and selection. *Cell* **129**, 147–161 (2007).
37. Vigorito, E. *et al.* microRNA-155 regulates the generation of immunoglobulin class-switched plasma cells. *Immunity* **27**, 847–859 (2007).
38. Chen, C.Z., Li, L., Lodish, H.F. & Bartel, D.P. MicroRNAs modulate hematopoietic lineage differentiation. *Science* **303**, 83–86 (2004).
39. Tan, L.P. *et al.* miRNA profiling of B-cell subsets: specific miRNA profile for germinal center B cells with variation between centroblasts and centrocytes. *Lab. Invest.* **89**, 708–716 (2009).
40. Ventura, A. *et al.* Targeted deletion reveals essential and overlapping functions of the miR-17 through 92 family of miRNA clusters. *Cell* **132**, 875–886 (2008).
41. Kang, S.G. *et al.* MicroRNAs of the miR-17-92 family are critical regulators of T(FH) differentiation. *Nat. Immunol.* **14**, 849–857 (2013).
42. Lu, Y.J. *et al.* Interleukin-17A mediates acquired immunity to pneumococcal colonization. *PLoS Pathog.* **4**, e1000159 (2008).
43. Malley, R. *et al.* $CD4^+$ T cells mediate antibody-independent acquired immunity to pneumococcal colonization. *Proc. Natl. Acad. Sci. USA* **102**, 4848–4853 (2005).
44. Trzcinski, K. *et al.* Protection against nasopharyngeal colonization by *Streptococcus pneumoniae* is mediated by antigen-specific $CD4^+$ T cells. *Infect. Immun.* **76**, 2678–2684 (2008).
45. Jaffar, Z., Ferrini, M.E., Herritt, L.A. & Roberts, K. Cutting edge: lung mucosal Th17-mediated responses induce polymeric Ig receptor expression by the airway epithelium and elevate secretory IgA levels. *J. Immunol.* **182**, 4507–4511 (2009).
46. Hirota, K. *et al.* Plasticity of Th17 cells in Peyer's patches is responsible for the induction of T cell-dependent IgA responses. *Nat. Immunol.* **14**, 372–379 (2013).
47. Wright, A.K. *et al.* Experimental human pneumococcal carriage augments IL-17A-dependent T-cell defence of the lung. *PLoS Pathog.* **9**, e1003274 (2013).
48. Du, C. *et al.* MicroRNA miR-326 regulates TH-17 differentiation and is associated with the pathogenesis of multiple sclerosis. *Nat. Immunol.* **10**, 1252–1259 (2009).
49. Chang, K.H., Mestdagh, P., Vandesompele, J., Kerin, M.J. & Miller, N. MicroRNA expression profiling to identify and validate reference genes for relative quantification in colorectal cancer. *BMC Cancer* **10**, 173 (2010).
50. Mizuno, H. *et al.* Identification of muscle-specific microRNAs in serum of muscular dystrophy animal models: promising novel blood-based markers for muscular dystrophy. *PLoS One* **6**, e18388 (2011).

Mucosal Immunization and Adjuvants

Hideki Hasegawa, Elly van Reit and Hiroshi Kida

Abstract The goal of the influenza vaccine is to prevent influenza virus infection and control the yearly seasonal epidemic and pandemic. However, the presently available parenteral influenza vaccine induces only systemic humoral immunity, which does not prevent influenza virus infection on the mucosal surface. Secretary IgA antibodies play an important role in preventing natural infection. Moreover, the IgA antibody response mediates cross-protection against variant viruses in animal models. Thus, a mucosal influenza vaccine that induces mucosal immunity would be a powerful tool to protect individuals from the influenza virus. Although the function of the mucosal immune system, especially in the respiratory tract, is not completely understood, there are several studies underway to develop mucosal influenza vaccines. Here, we will review current knowledge concerning the induction of IgA, the role of B-cell production of influenza virus specific IgA antibodies in anti-influenza immunity, and the role of humoral memory responses induced upon vaccination.

Contents

H. Hasegawa (✉) · E.van Reit
Department of Pathology, National Institute of Infectious Diseases, Toyama 1-23-1, Shinjuku, Tokyo 162-8640, Japan
e-mail: hasegawa@nih.go.jp

H. Kida
Research Center for Zoonosis Control, Hokkaido University, Sapporo, Japan

Current Topics in Microbiology and Immunology (2015) 386: 371–380
DOI: 10.1007/82_2014_402

Published Online: 12 July 2014

1 Introduction

Influenza viruses belong to the *Orthomyxoviridae* family, which is categorized into three genera, namely *influenzavirus A*, *B*, and *C*. *Influenzavirus A* comprise several subtypes based on the unique combination of two surface proteins, hemagglutinin (HA) and neuraminidase (NA). The seasonal influenza A virus infects millions of individuals each year, with the highest risk of complications occurring in young, elderly, and immunocompromised patients. For example, influenzavirus A can lead to fatal encephalopathy in infants and pneumonia in the elderly.

In addition, the avian and/or swine influenzavirus A has caused a pandemic every few decades by emerging each time as a genetically novel virus. The most recent pandemic in 2009 was caused by the influenzavirus A (H1N1) pdm09 of swine origin. Cases of highly pathogenic avian influenzavirus A H5N1 and H7N9 infection and fatal pneumonia have been also reported, with many individuals developing acute respiratory distress syndrome (ARDS) (La Gruta et al. 2007).

Vaccination is the most effective method to control both seasonal and newly evolved pandemic strains of the influenza virus. However, currently used parenteral influenza vaccines are only effective against strains that are closely antigenic to the vaccine strains. Thus, the yearly seasonal vaccine contains multiple influenza virus strains, including influenza virus A strains H1N1 and H3N2, and influenza virus B strain. However, there is an urgent need for improved cross-protection because antigenic mismatches between seasonal vaccines and circulating virus strains. It is also difficult to predict the newly evolved strains such as A/H5N1 and A/H7N9. Ideally, a universal influenza vaccine that induces a strong and long-lasting memory response and cross-protects against drifted variants, as well as against several subtypes of the influenza virus, which induce hetero-subtypic immunity, should be developed. While mucosal secretary IgA (S-IgA) antibodies show cross-protection against variant influenza viruses in mouse models, rational design of IgA antibody-inducing vaccines has so far been hampered by a lack of knowledge about local and tissue-specific immune responses and IgA antibody function (Matzinger and Kamala 2011). Consequently, the importance of IgA antibodies in immunity and the mechanisms by which IgA antibody responses are induced and maintained are just beginning to be established (Brandtzaeg 2007). In this review, we discuss the different mechanisms involved in the induction of S-IgA antibodies during influenza virus infection and vaccination and provide insight into how this information could be used to improve vaccine design.

2 The Use of Secretary IgA Antibodies for the Prevention of Influenza Virus Infection

The respiratory mucosal surface is the first line of defense against influenza virus infection. For example, pre-existing S-IgA antibodies on the surface of mucosal epithelial cells can eliminate a pathogen before it infects respiratory epithelial

cells, thereby providing immediate immunity (Renegar et al. 2004) in a process defined as immune exclusion (Stokes et al. 1975). S-IgA antibodies can also disarm viruses within infected secretory epithelial cells and redirect antigens to the lumen after they have entered the lamina propria (Brandtzaeg 2007). All of these responses are non-inflammatory in nature because, unlike IgG antibodies, IgA antibodies do not fix complement and do not activate the inflammatory complement pathway (Yel 2010). Therefore, a strong S-IgA response is critical for prevention of influenza virus infection especially in case of pathogenic strains for their severe clinical outcomes. Although it is difficult to study the functions of S-IgA and serum antibodies independently, mucosal vaccination and influenza virus infection in knockout mice, which lack poly Ig receptor expression and fail to secrete IgA antibodies from the mucosal surface, show that S-IgA antibodies protect against both homologous and heterologous influenza virus strains (Asahi et al. 2002, 2004). Moreover, transfer of S-IgA antibodies from respiratory tract washings from immunized to naïve mice has been shown to protect against challenge with a homologous or drifted strain (Tamura et al. 1991). Several studies in mice also have shown induction of strong homosubtypic, as well as modest heterosubtypic, cross-protective IgA antibodies.

Since the influenza vaccine is generally administered intramuscularly or subcutaneously, S-IgA antibodies are generally not produced in large quantities; however, intranasal and intradermal influenza vaccinations can produce an effective IgA antibody response (Amorij et al. 2010). The most common route for the influenza virus to enter the host is via the respiratory tract. Therefore, intranasal immunization is the most widely explored route of mucosal vaccination against influenza. FluMist® (MedImmune, LLC), a live attenuated influenza virus vaccine, is the only nasal vaccine on the market. However, the rational design of S-IgA vaccines has been hampered by a lack of knowledge on the mechanisms by which IgA antibodies are induced (Brandtzaeg 2007).

3 The Characteristics of IgA Antibodies

After IgG, IgA is the second most abundant isotype in the serum; however, approximately 70 % of all antibodies in mucosae are IgA (Macpherson et al. 2008). In the human serum, IgA antibodies are present mostly as monomeric IgA_1 (Yel 2010), while S-IgA antibodies are found as dimeric IgA_2, although tri- and tetrameric molecules also exist. These polymeric IgA antibodies consist of monomeric IgA molecules connected by one or more J (Joining) chains. After binding to the secretory component (SC), the ectodomain of the polymeric Ig receptor (pIgR), the polymeric IgA is secreted as S-IgA antibodies. Since the cross-protective characteristics of nasal IgA antibodies depend on the polymeric nature of IgA, understanding the molecular structure, development, and function of these higher order polymeric IgA antibodies may be important for the rational design of cross-protective vaccines (Taylor and Dimmock 1985; Song et al. 1995; Renegar et al. 1998).

IgA_2 antibodies develop mostly at sites colonized by a wide range of microbiota, including urogenital and distal intestinal tracts. For example, intestinal bacteria instruct dendritic cells (DC) to produce IgA antibodies (Massacand et al. 2008). IgA antibodies are also present in the respiratory tract, which is not populated with many commensals; however, the predominant isotype is IgA_1.

And IgA_1- specific proteases can cleave bonds within human IgA1 molecules, but these specific bonds are only present in IgA molecules in higher primates and not in the mouse (Weiser et al. 2003).

4 IgA Antibody Production in Mucosal Tissues

The inductive site of the mucosal immune system can be divided in two different sites, namely inductive and effector sites. The inductive site includes mucosa-associated lymphatic tissue (MALT), and local and regional draining lymph nodes. Antigens are directly taken from the mucosal surface with an important role of microfold (M) cells and antigen-presenting cells (APC). Antigen-specific antibody producing B-cells can be developed at two different inductive sites, namely extrafollicular and germinal centres (GC), and their induction involves T-cell-dependent or -independent mechanisms (Cerutti 2008). The GC is a specialized environment that supports affinity maturation, which is mediated by activation-induced deaminase (AID) induced somatic hypermutation (Honjo et al. 2004). In addition, AID participates in the production of the preferred antibody class by influencing class switch recombination (CSR) of the heavy chain (Honjo et al. 2004; Zaheen and Martin 2010). Most IgA memory B-cells (BMem) and long-lived IgA plasma cells develop in the GC of peripheral lymphoid organs and that step requires T-cell help via CD40L (CD154) and TGFβ1. T-cell-independent B-cell class switching in the GC might be mediated by interactions with (DC) and stromal cells, including follicular DC (Puga et al. 2010).

At extrafollicular mucosal sites, antibodies can develop both with and without the help of T-cells, with the latter process involving B-cell activating factor (BAFF) and a proliferation-inducing ligand (APRIL) (Chen and Cerutti 2010; Rothaeusler and Baumgarth 2010). Although hypermutation, which is necessary for affinity maturation, is minimal at these sites (MacLennan et al. 2003), antigen-specific antibody producing B-cells at this site can prevent reinfection (Lee et al. 2005) generate an IgG- and IgA-producing BMem subset (Berkowska et al. 2011).

IgA CSR mechanisms have been studied mostly in the gut where they are influenced by specific environmental factors that are mainly created by commensal bacteria and their products (Massacand et al. 2008). While the respiratory tract is not populated with as many commensals as the intestinal tract, it would appear to be protected from the influenza virus by commensals in the gut because CD4 and CD8 T-cell number and the IgA antibody response were reduced in mice treated with an antibiotic. Immunity against the influenza virus was restored by nasal administration of lipopolysaccharides (LPS) but also by rectal administration of

Toll-like receptor (TLR) agonists (e.g., LPS, CpG, polyI:C) (Ichinohe et al. 2011). These findings indicate that signals from distal mucosal regions can support immune priming in the mucosal effector in the respiratory tract. Additional studies are needed to determine whether distal regions contribute to immunity in the respiratory tract.

5 Innate Sensing and Mucosal Adjuvants

Influenza viruses activate pattern recognition receptors belonging to several different families, namely the TLR family, the RIG-I like receptor (RLR) family, the Nod-like receptor (NLR) family (Pang and Iwasaki 2011), and the C-type lectin family (Londrigan et al. 2011). To improve vaccine efficacy, members of the pattern recognition receptor family, which are not activated by influenza virus infection, can be employed. For example, flagellin, which activates TLR5, promotes IgA production and heterosubtypic protection when incorporated into the membrane of influenza virus-like particles (Wang et al. 2010). Similarly, PolyI:$PolyC_{12}U$, activating TLR3, has been shown to induce heterosubtypic protection through IgA antibodies after administration of an intranasal vaccine (Ichinohe et al. 2007). Moreover, the TLR3 ligand acts synergistically with the TLR-2 ligand zymosan (Ainai et al. 2010).

Recently, several models have demonstrated the importance of TLR signaling in CSR. Early studies have shown only two signals to induce CSR in naïve B-cells, namely, the presentation of antigenic peptides on MHC class II molecules after antigen binding to the B-cell receptor, and the activation of these B-cells via cytokines and the interaction of CD40-CD40L with antigen-specific T-cells. Presently, TLR signaling is thought to involve an important third signal (Bekeredjian-Ding and Jego 2009). A recent study has shown that MyD88 can induce a protective immune response during primary, but not secondary, influenza virus infection. The IgA level in MyD88-/-TRIF-/- mice is reduced in the saliva during secondary infection; however, in serum and nasal wash, the level, which was induced in a TLR-independent manner, is similar to those in wild type mice (Seo et al. 2010). Furthermore, TLRs play a role in both T-cell-dependent and -independent IgA responses in mucosal and systemic antibody levels (Bessa et al. 2009).

Some APCs such as plasmacytoid DCs (pDC), Tip-DCs (TNF and Inducible nitric oxygen species (iNOS) Producing DC) and LAPCs have been reported to with the IgA response. In addition, pDCs trigger the anti-influenza response by inducing type 1 interferon, Th1, and cytotoxic responses and enhancing B-cell expansion and differentiation into CD27 high plasmablasts upon TLR7 stimulation (Douagi et al. 2009). pDCs are also necessary for optimal mucosal IgA and serum IgG production after primary, but not secondary, booster influenza vaccination, live attenuated virus vaccination, and inactivated whole virus or split virus vaccination. By contrast, pDCs are not needed to induce an immune response to a live virus (Koyama et al. 2010).

Upon infection of highly pathogenic influenza virus strains, Tip-DCs produce large concentrations of both tumor necrosis factor (TNF) and nitric oxide (NO), which results in tissue damage (Aldridge et al. 2009). However, controlled concentrations of NO induce TGF-βRII expression by B-cells, thereby enabling T-cell dependent IgA class switching. MyD88 signaling downstream of TLR2, 4, and/or 9, which is critical for the induction of iNOS, facilitates T-cell-independent IgA secretion in BAFF- and APRIL-dependent manners (Tezuka et al. 2007).

Late-activator APC (LAPC), a newly identified APC, may play an important role in the immune response several days after influenza virus infection. While the influenza virus activates DCs at approximately 3 days after infection and induces Th1-type responses, the LAPC is activated at approximately 8 days after infection. This results in the induction of a Th2-type response, production of IgA, IgG_1 and IgG_2 antibodies, and downregulation of the anti-viral Th1-type response (Yoo et al. 2010).

6 Mucosal Vaccine Design

Currently used seasonal influenza vaccines are produced based on the prediction of strains that might cause an epidemic in the following season. These vaccines are generally injected intramuscularly or subcutaneously, and are expected to reduce the severity of the disease caused by specific strains that are homologous to the vaccine strain. These vaccines neither induce cross-protection against the heterologous strain nor prevent infection because they largely induce neutralizing IgG antibodies in the serum. On the other hand, influenza vaccines currently under design aim to induce broader cross-protection and are referred to as 'universal influenza vaccines'. The more diverse and broader cross-protective immune response induced by natural infection than by current parenteral vaccinations suggests the induction of several possible immunological effectors that add to cross-protection. Furthermore, individuals of different genders, ages, and genetic backgrounds respond differently to vaccines; thus, they may rely on different immune mediators for their protection (Nayak et al. 2010; McKinstry et al. 2011).

While infection with the natural influenza virus is superior to vaccination in inducing cross-protection against infection by mutated viruses within a particular subtype of the A-type virus in humans (Hoskins et al. 1976, 1979; Couch and Kasel 1983), an inactivated whole virus particle vaccine has been shown to be more immunogenic than split vaccines. This is in agreement with the general view that the effectiveness and safety of vaccines are usually inversely correlated.

Both inactivated whole virion vaccines and split seasonal vaccines can induce protective immune responses against the homologous virus (Greenbaum et al. 2004). While heterosubtypic immunity is not observed after administration of an ether-split vaccine, an inactivated whole virion vaccine can induce broad heterosubtypic immunity (Takada et al. 2003). The stronger immunogenicity of the inactivated whole virion vaccine in mice is likely due to the stimulation of innate

immunity by genomic single-stranded RNA via TLR7 (Diebold et al. 2004; Lund et al. 2004). Since most viruses produce dsRNA during replication (Jacobs and Langland 1996), synthetic dsRNA can likely act as a partial molecular mimic of viral infection.

This has been confirmed in a previous study where intranasal administration of an ether-split vaccine from PR8 (a H1N1 influenza virus strain) and poly(I:C), a TLR3 agonist adjuvant, induced a strong anti-HA IgA and IgG response in nasal washes and serum, respectively, while vaccination without poly(I:C) induced a weak response. In addition, administration of either an A/Beijing (H1N1) or A/Yamagata (H1N1) vaccine, which are antigenically different from A/PR8, in the presence of poly(I:C) confered complete protection against A/PR8 virus challenge in a mouse model of nasal infection, indicating that intranasal vaccination with poly(I:C) adjuvant confers cross-protection against variant viruses (Ichinohe et al. 2005). Safety issue of the adjuvant is very important. One of dsRNA poly(I:C_{12}U)(Ampligen) which are clinically safe were recently shown to be a potent inducer of innate immune responses (Caskey et al. 2011). This dsRNA, poly(I:C12U)(Ampligen), was investigated as a dsRNA adjuvant for intranasal avian influenza vaccines (Ichinohe et al. 2009).

The stronger immunogenicity produced by the live virus than by the whole inactivated virus may be caused by a mechanism that does not involve stimulation of TLR7 or 3. For example, other receptors, or a different biodistribution or kinetic profile may be involved. For inactivated vaccine the former might be mimicked by using a ligand for TLRs as an adjuvant, the latter two might possibly be mimicked by the use of different carriers for the antigens that will influence kinetics as well as biodistribution (Bachmann and Jennings 2010).

While investigators continue to understand infections caused by the influenza virus, the ultimate goal is to produce a vaccine that can overcome natural infections. This might be achieved by carefully selecting highly conservative domains within influenza membrane proteins and using them as vaccines in combination with several adjuvants which could activate a broad spectrum of tissues and cells.

A recent clinical study reported that intranasal administration of a whole inactivated influenza virus without adjuvant but with a prime-booster induced high levels of nasal neutralizing antibodies that consisted primarily of polymeric IgA (Ainai et al. 2013). It is not clear whether the absence of adjuvant was not important for eliciting the antibody response in these subjects who would have had a cross-protective memory resulting from a history of infections and/or vaccinations.

In conclusion, the induction of IgA antibodies after vaccination can enhance the immune response by introducing a local immune response, which adds to cross-protection, balances pro-inflammatory responses, and increases the diversity of immunological memory. The fact that IgA antibodies alone cannot induce complete protection after heterosubtypic infection may be an advantage because partial protection by IgA antibodies can reduce the viral load and provide time for immune system priming. In this way, innate, humoral, and cellular responses are activated, resulting in the strongest renewal of immunological memory. This ensures the best possible preparedness for the next influenza virus encountered.